





# SEMI-ROLLED LEAF 10 stabilizes catalase isozyme B to regulate leaf morphology and thermotolerance in rice (*Oryza sativa* L.)

Jiajia Wang<sup>1,2,+,#</sup>, Jing Xu<sup>1,3,+,#</sup> , Li Wang<sup>1</sup>, Mengyu Zhou<sup>1</sup>, Jinqiang Nian<sup>1</sup>, Minmin Chen<sup>1</sup>, Xueli Lu<sup>1</sup>, Xiong Liu<sup>1</sup>, Zian Wang<sup>1</sup>, Jiangsu Cen<sup>1</sup>, Yiting Liu<sup>1</sup>, Zhihai Zhang<sup>1</sup>, Dali Zeng<sup>1</sup>, Jiang Hu<sup>1</sup>, Li Zhu<sup>1</sup>, Guojun Dong<sup>1</sup>, Deyong Ren<sup>1</sup>, Zhenyu Gao<sup>1</sup>, Lan Shen<sup>1</sup>, Qiang Zhang<sup>1</sup>, Qing Li<sup>1</sup>, Longbiao Guo<sup>1</sup>, Sibin Yu<sup>2</sup> , Qian Qian<sup>1,4,5,\*</sup>  and Guangheng Zhang<sup>1,4,5,\*</sup> 

<sup>1</sup>State Key Laboratory of Rice Biology, China National Rice Research Institute, Hangzhou, China

<sup>2</sup>National Key Laboratory of Crop Genetic Improvement and National Center of Plant Gene Research, College of Plant Science and Technology, Huazhong Agricultural University, Wuhan, China

<sup>3</sup>State Key Laboratory of Tree Genetics and Breeding, Key Laboratory of Tree Breeding of Zhejiang Province, Research Institute of Subtropical Forestry, Chinese Academy of Forestry, Hangzhou, China

<sup>4</sup>Hainan Yazhou Bay Seed Laboratory, Sanya, China

<sup>5</sup>National Nanfan Research Institute (Sanya), Chinese Academy of Agricultural Sciences, Sanya, China

Received 10 March 2022;

revised 18 December 2022;

accepted 25 December 2022.

\*Correspondence (Tel: +86 571 63371418;

fax: +86 571 63370389; email

qianqian188@hotmail.com; Tel: +86 571

63439178; fax: +86 571 63370389; email

zhangguangheng@126.com)

<sup>†</sup>These authors contributed equally to this work.

<sup>‡</sup>co-first authors.

## Summary

Plant architecture and stress tolerance play important roles in rice breeding. Specific leaf morphologies and ideal plant architecture can effectively improve both abiotic stress resistance and rice grain yield. However, the mechanism by which plants simultaneously regulate leaf morphogenesis and stress resistance remains elusive. Here, we report that *SRL10*, which encodes a double-stranded RNA-binding protein, regulates leaf morphology and thermotolerance in rice through alteration of microRNA biogenesis. The *sr10* mutant had a semi-rolled leaf phenotype and elevated sensitivity to high temperature. *SRL10* directly interacted with catalase isozyme B (CATB), and the two proteins mutually increased one other's stability to enhance hydrogen peroxide (H<sub>2</sub>O<sub>2</sub>) scavenging, thereby contributing to thermotolerance. The natural Hap3 (AGC) type of *SRL10* allele was found to be present in the majority of *aus* rice accessions, and was identified as a thermotolerant allele under high temperature stress in both the field and the growth chamber. Moreover, the seed-setting rate was 3.19 times higher and grain yield per plant was 1.68 times higher in near-isogenic line (NIL) carrying Hap3 allele compared to plants carrying Hap1 allele under heat stress. Collectively, these results reveal a new locus of interest and define a novel *SRL10*–CATB based regulatory mechanism for developing cultivars with high temperature tolerance and stable yield. Furthermore, our findings provide a theoretical basis for simultaneous breeding for plant architecture and stress resistance.

**Keywords:** rice (*Oryza sativa* L.), microRNA, leaf morphology, catalase isozyme B (CATB), thermotolerance.

## Introduction

Rice yield is closely linked to both plant architecture and stress resistance. The two 'Green Revolutions' and super-rice breeding programs are based on continuous improvement of these two characteristics (Guo *et al.*, 2020). To capitalize on available resources and maximize seed setting, plants make constantly adjustments in response to changes in environmental factors (Xu *et al.*, 2021). Certain architectures, can predispose plants for success under specific conditions. For example, upright plant architecture facilitates high-density planting (Tian *et al.*, 2019), whereas a semi-dwarf architecture can enhance lodging resistance and crop yield (Guo *et al.*, 2021; Liu *et al.*, 2018; Wang and Li, 2005). Appropriate leaf rolling not only contributes to enhanced light penetration into the canopy (Chen *et al.*, 2019b; Sun *et al.*, 2020; Xu *et al.*, 2018) but also helps to improve root system activity and strengthen lodging resistance (Sun *et al.*, 2020; Zhang *et al.*, 2009; Zou *et al.*, 2011). Extreme climate events have huge negative impact on global food production (Ray *et al.*, 2015); for crops that are vulnerable to

temperature fluctuations, precise control over heat resistance will be necessary in the future to minimize plants damage (Mittler *et al.*, 2012). It is therefore of great practical significance for rice production to cultivate new germplasm resources with beneficial leaf morphologies and enhanced heat tolerance.

Stages of leaf development include leaf initiation, polarity establishment and maintenance, leaf flattening and intercalary growth (Du *et al.*, 2018). Leaf morphology is determined by polarity along three axes: adaxial–abaxial, medial–lateral and apical–basal (Hasson *et al.*, 2010; Moon and Hake, 2011). Establishment of leaf polarity is the result of complex interaction between regulatory networks involving phytohormone signalling pathways, transcription factors and microRNAs (miRNAs) (Wang *et al.*, 2020a; Xu *et al.*, 2018). Significant progress has been made in recent years towards the mechanisms that regulate leaf morphology; many relevant genes have been identified in rice, such as *SHALLOT-LIKE1* (*SLL1*) (Zhang *et al.*, 2009) and *SLL2* (Zhang *et al.*, 2015b), *ABAXIALLY CURLED LEAF 1* (*ACL1*) (Li *et al.*, 2010), *SEMI-ROLLED LEAF 1* (*SRL1*) (Li *et al.*, 2017; Xiang *et al.*, 2012;) and *SRL2* (Liu *et al.*, 2016), Class III HD-Zip

gene *HOMEODOMAIN CONTAINING PROTEIN 4 (OSHB4)* (Li et al., 2016b), *ARGONAUTE-1 (AGO1) ISOFORMS B (AGO1b)* (Li et al., 2019), and members of the *RICE OUTERMOST CELL-SPECIFIC GENE (Roc)* family *Roc8* and *Roc5* (Fang et al., 2021; Sun et al., 2020). Many genes have pleiotropic effects in regulating stress resistance, plant architecture and nutrient utilization; examples include *PHOTO-SENSITIVE LEAF ROLLING 1 (PSL1)* (Zhang et al., 2021a), *SLL1* (Zhang et al., 2009), *DENSE PANICLE 1 (DEP1)/qLL9* (Fu et al., 2019; Huang et al., 2009), *IDEAL PLANT ARCHITECTURE 1 (IPA1)* (Lu et al., 2013; Springer, 2010; Wang et al., 2021b) and *DWARF 1 (D1)/LW5* (Fujisawa et al., 1999; Zhu et al., 2020). *PSL1* is known to modify cell wall structure and drought tolerance in rice (Zhang et al., 2021a), whereas *D1* is involved in a complex network regulating plant height, leaf size and abiotic stress responses (Fujisawa et al., 1999; Jangam et al., 2016; Zhu et al., 2020).

Heat stress causes different degrees of damage to protein, membrane, RNA and cytoskeleton, and changes the efficiency of intracellular reactions, leading to metabolic imbalances (Vu et al., 2019). Many genes regulated thermotolerance through complex regulatory networks involving the rapid plasma membrane (PM) sensing mechanism,  $Ca^{2+}$  signal transduction, reactive oxygen species (ROS) metabolism, post-transcriptional RNA modifications, ubiquitinated protein degradation and the unfolded protein response (UPR) in the endoplasmic reticulum (ER) and cytosol (Mittler et al., 2012). Genes involved in these processes include *SLENDER GUY 1 (SLG1)* (Xu et al., 2020), *ADAPTATION TO ENVIRONMENTAL TEMPERATURE 1 (AET1)* (Chen et al., 2019a), the NOP/Sun family members *NSUN2* (Tang et al., 2020), *THERMO-TOLERANCE 1 (TT1)* (Li et al., 2015), *TT2* (Kan et al., 2022) and *HIGH TEMPERATURE SENSITIVE 1 (HTS1)* (Chen et al., 2021). Although many regulatory genes that influence leaf morphology or thermotolerance have been identified, there are few reports detailing combined analyses of leaf morphology and thermotolerance. Identifying genes that simultaneously regulate both leaf morphology and stress resistance should clarify the mechanisms by which these regulatory pathways are integrated and provide new avenues for breeding high-yield, high-quality rice varieties in the future.

In plants, proteins that contain double-stranded RNA-binding motifs (dsRBMs) play integral roles in small RNA biosynthesis (Raghuram et al., 2015). Moreover, dsRBMs are also known to be important in plant development and defence (Bartel and Bartel, 2003; Hiraguri et al., 2005; Waterhouse et al., 2001). Twelve dsRBM-containing proteins have been identified in rice, including eight double-stranded RNA-binding (DRB) proteins and four Dicer-like (DCL) proteins. Functional analysis of DCLs (such as *OsDCL1*, *OsDCL3b* and *OsDCL4*) has suggested that dsRBM-containing proteins have critical roles in leaf morphology (Liu et al., 2005), small RNA biogenesis (Song et al., 2012) and basal resistance against rice blast disease (Zhang et al., 2015a). However, few members of DRBs family have been functionally characterized in rice. Moreover, there have been no reports of DRBs simultaneously regulating of plant architecture and stress resistance.

In the present study, we identified a rice mutant that displayed increased temperature sensitivity and a semi-rolled leaf phenotype. The causal gene, named *SRL10*, encoded a dsRBM-containing protein and regulated miRNA biogenesis. *SRL10* not only affected leaf morphology, but also increased thermotolerance by interacting with catalase isozyme B (CATB) and enhancing the  $H_2O_2$  scavenging ability of CATB. Natural variations in

*SRL10* confer differential degrees of thermotolerance to *japonica*, *indica* and *aus* cultivars; the Hap3 (AGC) allele of *SRL10*, which was prevalent in the majority of *aus* rice, was identified as a thermotolerant haplotype. We therefore propose that manipulation of *SRL10* has potential applications in super-high-yield rice breeding by simultaneously improving plant architecture and stress resistance.

## Results

### Phenotypic characterization of the *srl10* mutant

The *srl10* mutant, identified in a screen of an ethyl methane-sulfonate (EMS) mutant library in the 'Wuyunjing 7' (WYJ7) background, was sensitive to heat stress (Figure 1c,d) and had adaxially rolled leaves throughout the entire growth period (Figure 1a, 7a,b). The leaf rolling index (LRI) of *srl10* at the tillering stage was approximately 36.22%, whereas WYJ7 leaves were nearly flat, with an average LRI of 0.82% (Figure 1g). Moreover, *srl10* plants had twice as many bulliform cells (BCs) as WYJ7, and the BC area was 2.5 times larger (Figure 1b,e,f). These results suggested that the increased BC number and size may have been responsible for the observed adaxial leaf rolling in *srl10*. In response to heat stress, both WYJ7 and *srl10* at seedling stage or tillering stage showed leaf damage in the form of twisted leaf tips, but less change in LRI (Figure 1c,d,i). *srl10* plants had a significantly lower survival rate than WYJ7 plants under heat stress (Figure 1h). In addition, transcriptomic analysis revealed 118 differentially expressed genes (DEGs) related to heat stress responses between WYJ7 and *srl10*; these DEGs were primarily enriched in functions related to protein processing in ER (Figure S1d,e). Moreover, *SRL10* was strongly induced by heat and abscisic acid (ABA) treatment (Figure S1f,g), suggesting that *SRL10* is involved in regulation of thermotolerance.

Cell wall structure, stomata morphology, leaf water content and leaf water loss rate are all closely related to the transpiration rate (Zhang et al., 2015b; Zhang et al., 2021a). We therefore tested these parameters in WYJ7 and *srl10* plants. Water loss rates in isolated leaves were significantly lower in *srl10* compared to WYJ7 plants (Figure 2c); the leaf water content of *srl10* was 71.02%, which was 1.76% higher than that of WYJ7 (Figure 2d). Moreover, the BC walls were 2.3 times thicker in *srl10* than in WYJ7 (Figure 2a,e). This was consistent with the differences observed in levels of cell wall components (namely cellulose, hemicellulose and pectin) between WYJ7 and *srl10* leaves (Figure 2f-h). In addition, stomatal apertures were markedly smaller in *srl10* than WYJ7 (Figure 2b,i,j), consistent with observed decreases in transpiration rate and stomatal conductance in *srl10* plants (Figure 2l,m). These results suggested that abnormal development of leaf histocytes leads to changes in leaf physiological characteristics. Furthermore, analysis of yield-trait performance in WYJ7 and *srl10* showed that loss of *SRL10* function resulted in significant decreases in grain filling rate (Figure 3d), 1000-grain weight (Figure 3e), grain yield (Figure 3f), number of secondary branches (Figure 3l), grain numbers per panicle (Figure 3j) and photosynthetic rate (Figure 2k). Taken together, these results demonstrated that *SRL10* had pleiotropic effects on rice growth and development.

### Map-based cloning of *SRL10*

The semi-rolled leaf phenotype was used as the mapping trait to identify the underlying genetic basis. Genetic analysis indicated

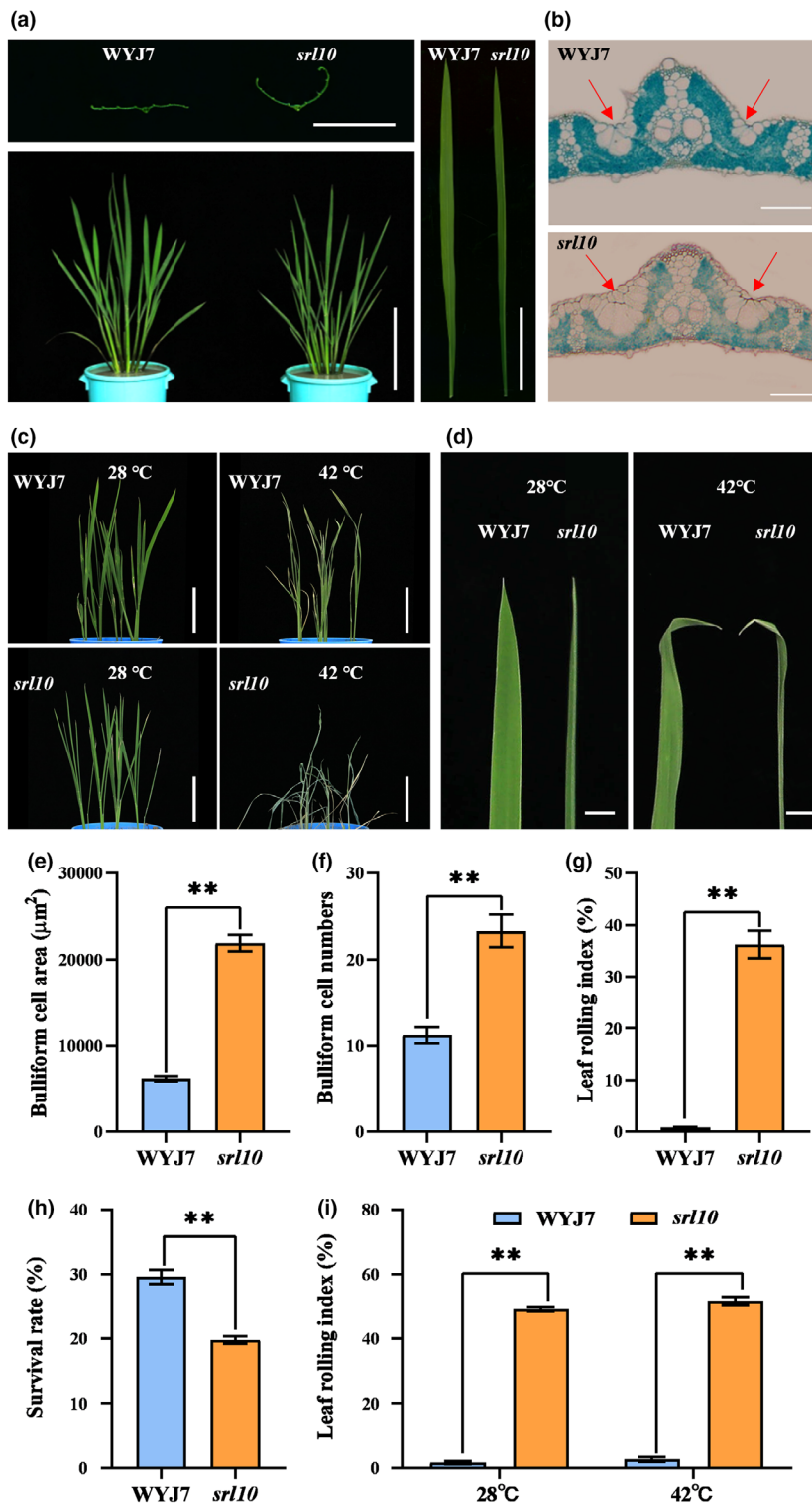


**Figure 1** Phenotypic comparison of WYJ7 and *srl10*. (a) Representative images of WYJ7 and *srl10* transverse leaf sections (upper left), whole leaves (right) and whole plants (lower left) at the tillering stage. Scale bars = 1.5 cm, 10 cm and 20 cm respectively. (b) Paraffin sections of WYJ7 and *srl10* leaves. Red arrows represent bulliform cells (BCs). Scale bar = 100  $\mu\text{m}$ . (c) Representative WYJ7 and *srl10* plants at seedling stage grown at 28 °C (left) or 42 °C (right), Scale bar = 2.5 cm. (d) Representative WYJ7 and *srl10* leaves at tillering stage grown at 28 °C (left) or 42 °C (right), Scale bar = 1 cm. (e, f) The areas (e) and numbers (f) of bulliform cells in WYJ7 and *srl10*. (g) Leaf rolling index (LRI) of WYJ7 and *srl10* at tillering stage. (h) Survival rates of WYJ7 and *srl10* plants. (i) Leaf rolling index (LRI) of WYJ7 and *srl10* leaves grown at 28 °C or 42 °C. Data are shown as mean  $\pm$  standard deviation. Asterisks indicate significant difference based on the Student's *t* test: \*\* for  $P < 0.01$ ; ns, not significant.

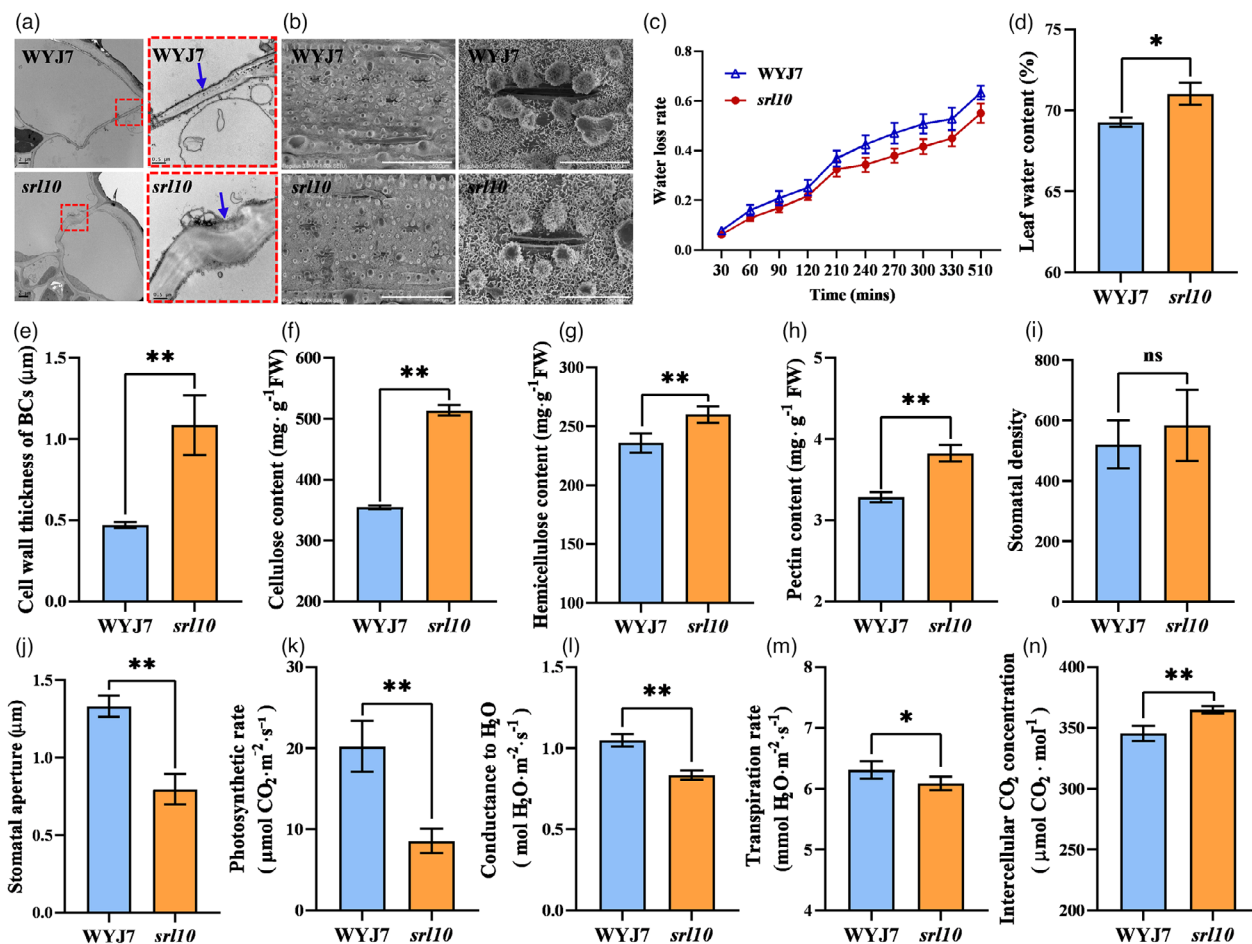


**Figure 2** Investigation of physiological characters of WYJ7 and *srl10*. (a) Micrographs showing BC walls in WYJ7 and *srl10* leaves. Regions outlined in red are shown in greater detail at right. Blue arrows indicate BC walls. Scale bar = 2  $\mu\text{m}$  (left) and 0.5  $\mu\text{m}$  (right). (b) Micrographs of stomatal morphology in WYJ7 and *srl10* leaves. Scale bar = 50  $\mu\text{m}$  (left) and 10  $\mu\text{m}$  (right). (c) Water loss rate of detached leaves in WYJ7 and *srl10*,  $n = 5$ . (d) Leaf water content of WYJ7 and *srl10*,  $n = 5$ . (e) Cells wall thickness of BC in leaves of WYJ7 and *srl10*. (f–h) The level of cell wall component in leaves of WYJ7 and *srl10*: (f) Cellulose content; (g) Hemicellulose content; (h) Pectin content,  $n = 5$ . (i,j) Stomatal density per  $\text{mm}^2$  (i) and stomatal aperture (j) in leaves of WYJ7 and *srl10*. (k–n) Photosynthetic characteristics of WYJ7 and *srl10*. (k) Photosynthetic rate, (l) conductance to  $\text{H}_2\text{O}$ , (m) transpiration rate and (n) intercellular  $\text{CO}_2$  concentration of WYJ7 and *srl10*,  $n = 10$ . Data are given as mean  $\pm$  standard deviation. Asterisks indicate significant difference based on the Student's *t* test: \* for  $P < 0.05$ ; \*\* for  $P < 0.01$ ; ns, not significant.

that the semi-rolled leaf phenotype of *srl10* was determined by a single recessive nuclear gene (Table S1). We mapped the locus to a 27.04-kb interval between the simple sequence repeat (SSR) markers C10-2 and C10-3. This interval contained two putative open reading frames (ORFs), *LOC\_Os10g33970* and *LOC\_Os10g33980* (Figure 4a). DNA sequence analysis of these putative ORFs revealed the presence of a single nucleotide substitution (C  $\rightarrow$  T) in the 29th base after ATG in the first exon of *LOC\_Os10g33970* in *srl10* compared to the wild type (Figure 4a,e), which resulted in an Ala-to-Val substitution. We therefore inferred that *LOC\_Os10g33970* was the gene controlling the *srl10* mutant phenotype.

To confirm this hypothesis, we carried out a complementation assay, expressing *LOC\_Os10g33970* in the *srl10* background (Figure 4b). The LRI values and survival rates of *SRL10*-complementation (*SRL10*-COM) plants did not differ from the wild type (Figure 4b–d,h,i). These results showed that the normal functioning of *LOC\_Os10g33970* in *srl10* recovered wild-type

characteristics in the *srl10* background. Furthermore, we overexpressed *LOC\_Os10g33970* in the WYJ7 background and obtained three independent transgene-positive  $T_2$  lines. All three independent lines expressed *LOC\_Os10g33970* at significantly higher levels, and displayed abaxially rolled flag leaves with decreased BC number and area compared to WYJ7 (Figure 5b–d; Figure S2). Moreover, the LRI of abaxially rolled leaves increased along with *SRL10* expression levels (Figure S2c,d).

We then generated three independent *LOC\_Os10g33970* knockout lines in the Nipponbare background with CRISPR/Cas9 (Figure 5e–h; Figure S3). The three lines contained 1-bp, 2-bp and 4-bp deletions respectively (Figure S3), in the third exon of *LOC\_Os10g33970*, which resulted in frameshift mutations. All three lines showed semi-rolled leaves and increased BC numbers (Figure 5f–h), a combination similar to our observations in *srl10*. Thus, the phenotypes of both overexpression and loss-of-function plants indicated that *LOC\_Os10g33970* was a key regulator of leaf rolling and that mutation of this gene caused the



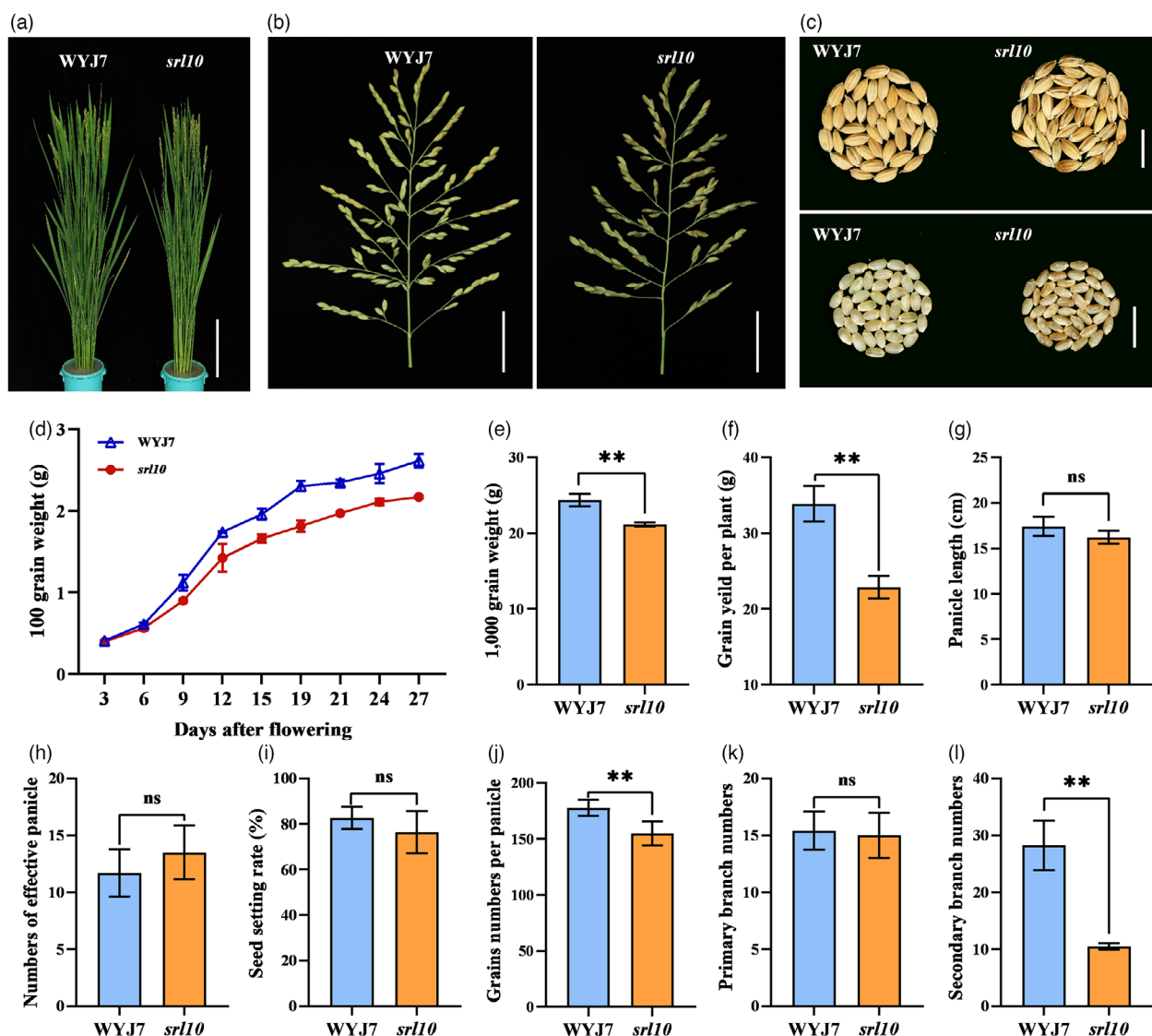


**Figure 3** Yield-trait performance of WYJ7 and *srl10*. (a) Plant morphology of WYJ7 and *srl10* at the mature stage, bar = 20 cm. (b) Spike morphology of WYJ7 and *srl10*. Scale bar = 3 cm. (c) Representative grain size (upper) and brown rice size (lower) of WYJ7 and *srl10*. Forty grains are shown per sample. Scale bar = 1 cm. (d) Grain filling dynamic of WYJ7 and *srl10*. (e–l) Statistical analysis of yield-trait between WYJ7 and *srl10*: 1000-grain weight (e), grain yield per plant (f), panicle length (g), numbers of effective panicles (h), seed-setting rate (i), grain numbers per panicle (j), primary branch numbers per panicle (k) and secondary branch numbers per panicle (l) of WYJ7 and *srl10*. Data are given as mean  $\pm$  standard deviation. Asterisks indicate significant difference based on the Student's *t* test: \*\* for  $P < 0.01$ ; ns, not significant.

temperature-sensitive and semi-rolled leaf phenotypes of *srl10*. We therefore designated *LOC\_Os10g33970* as *SRL10*.

*SRL10* consisted of three exons and two introns, and was predicted to encode a DRB protein. Phylogenetic analysis demonstrated high similarity between rice *SRL10* and homologues in *Zea mays* (71.05% sequence similarity), *Glycine max* (65.23%), *Arabidopsis thaliana* (63.92%), *Oryza brachyantha* (92.73%), *Sorghum bicolor* (72.16%) and *Hordeum vulgare* (72.50%) (Figure S4a,b). These findings demonstrated that *SRL10* was conserved between monocotyledonous and dicotyledonous angiosperms, and is therefore likely to have a fundamental function in plants. The *Arabidopsis* homologue, *AtDRB2*, is required for miRNA biogenesis (Eamens *et al.*, 2012). We therefore hypothesized that *SRL10* may be involved in regulation of miRNA biosynthesis in rice. To confirm this hypothesis, we

performed small RNA-seq analysis and found significant differences in accumulation of miR166m, miR399d and miR399j between WYJ7 and *srl10*, consistent with the results of quantitative reverse transcription PCR (qRT-PCR) (Figure 4f,g,j). While there was no significant difference in the accumulation of miR166m between WYJ7 and *SRL10-OE* (Figure S6a). These results suggested that loss of *SRL10* function affected miRNA biosynthesis.

Next, a  $\beta$ -glucuronidase (GUS) reporter system was used to identify tissues expressing *SRL10*. Strong GUS signals were observed in the seedlings, roots, stems, leaves, leaf sheaths and panicles (Figure 5j), consistent with *SRL10* expression levels in those tissues measured with qRT-PCR (Figure 5k). A green fluorescent protein (GFP)–*SRL10* fusion system was then used to determine the subcellular localization of *SRL10*, and the

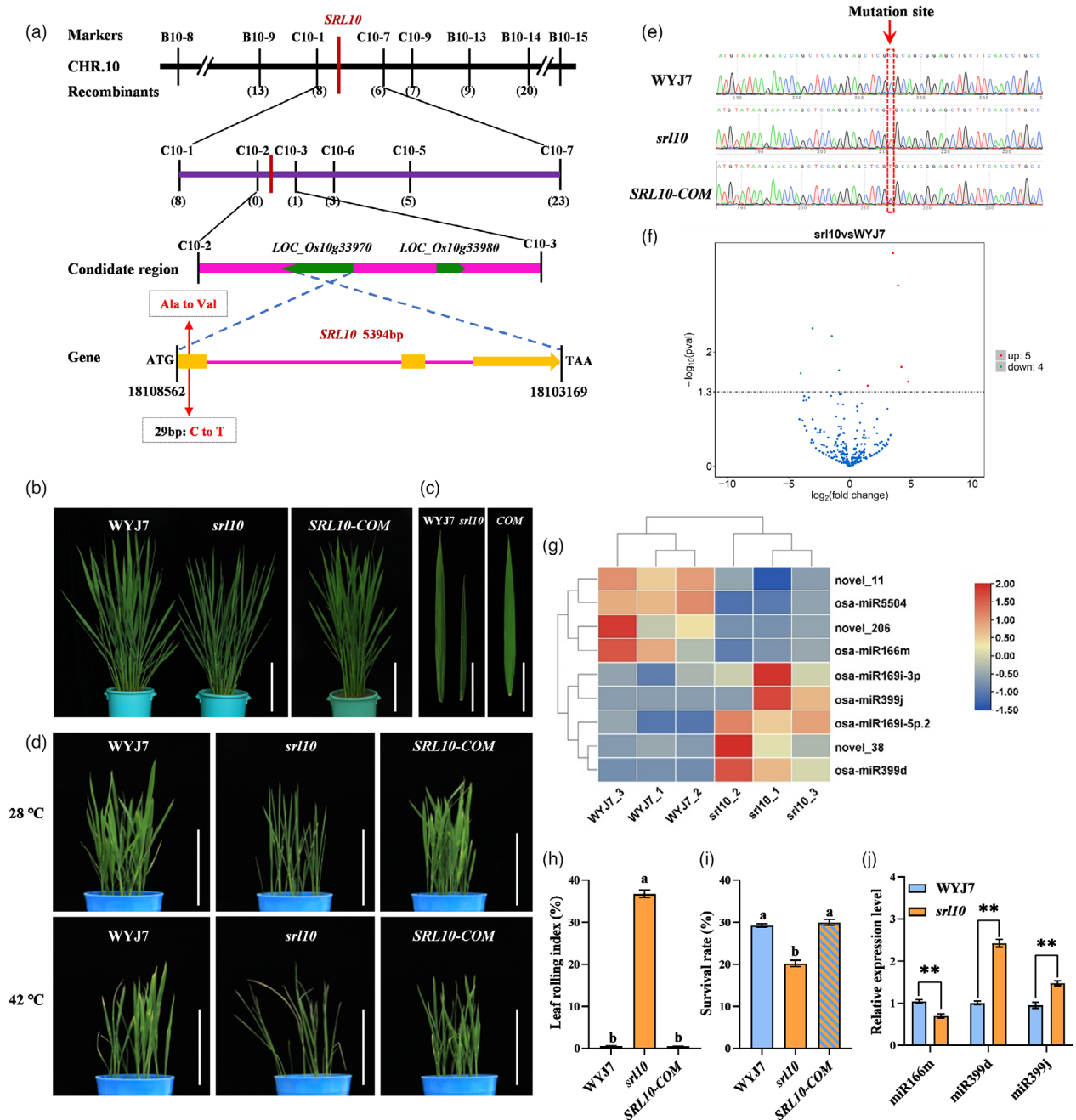


**Figure 4** Map-based cloning of *SRL10*. (a) Mapping of *SRL10*. (b–d) Complementation tests of *SRL10*. Representative images of WYJ7, *srl10* and *SRL10-COM* ( $T_2$ -generation) plants (b) and leaves (c) under standard growth conditions. Scale bars = 20 cm and 7 cm respectively. (d) WYJ7, *srl10* and *SRL10-COM* plants under standard growth conditions (upper) and heat stress (lower). Scale bar = 5 cm. (e) Chromatograms showing the sequences of WYJ7, *srl10* and *SRL10-COM* in the relevant region of *LOC\_Os10g33970*. (f) Volcano plot of differentially expressed miRNAs between WYJ7 and *srl10*. (g) Heat map of differentially expressed miRNAs between WYJ7 and *srl10*. (h) Leaf rolling index (LRI) values of WYJ7, *srl10* and *SRL10-COM*. Data are given as mean  $\pm$  standard deviation. Significant differences between groups are marked with different letters (Duncan's multiple range test,  $P < 0.05$ ). (i) Survival rate of WYJ7, *srl10* and *SRL10-COM* after heat stress. Data are given as mean  $\pm$  standard deviation. Significant differences between groups are marked with different letters (Duncan's multiple range test,  $P < 0.05$ ). (j) Relative expression level of miR166m in leaves of WYJ7 and *srl10*. Data are given as mean  $\pm$  standard deviation. Asterisks indicate significant difference based on the Student's *t* test: \*\* for  $P < 0.01$ .

fluorescent signal was primarily observed in the cytoplasm (Figure 5). These results indicated that *SRL10* was ubiquitously expressed in different tissues and *SRL10* protein was primarily localized to the cytoplasm.

#### *SRL10* interacted with *CATB*

To uncover the genetic pathway involved in *SRL10* regulation, we performed a yeast two-hybrid (Y2H) screen of a rice cDNA library.

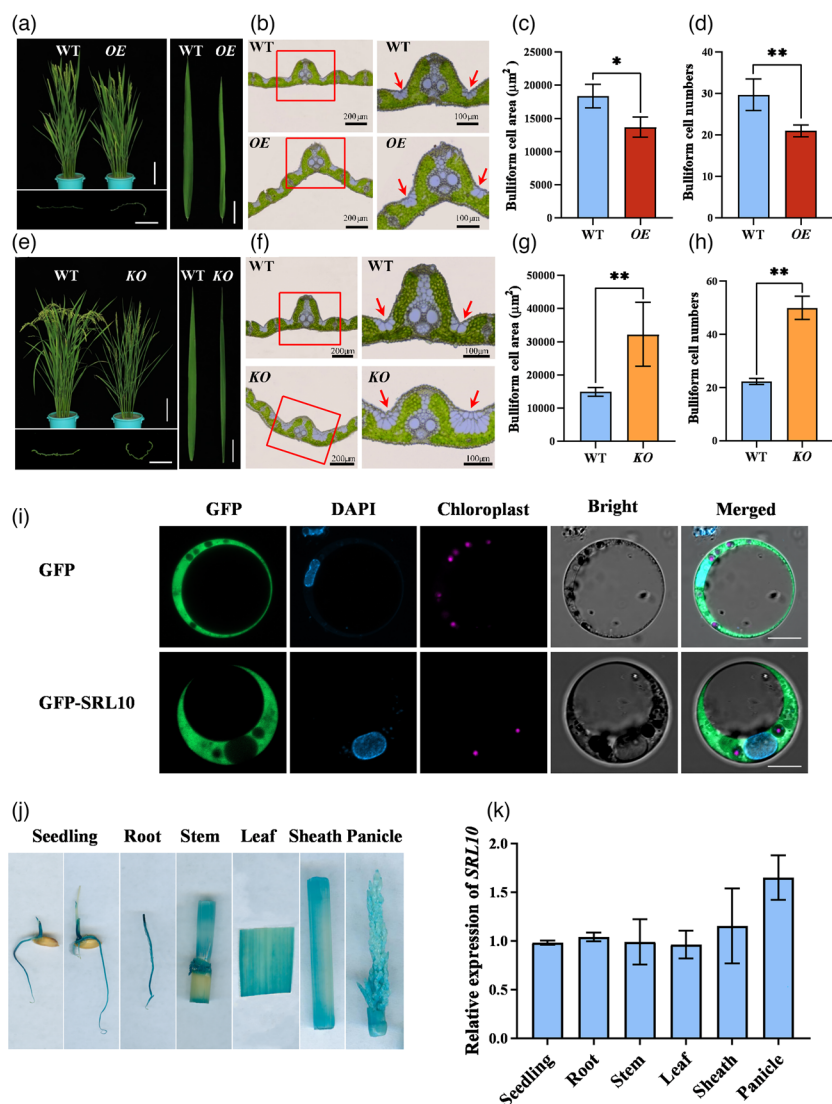


**Figure 5** Functional verification of *SRL10*. (a–d) Overexpression tests of *SRL10*. (a) Representative images of WYJ7 (WT) and *SRL10*-overexpression (OE) whole plants (upper left), leaves (right) and leaf cross-sections (lower left). Scale bars = 20 cm, 2.5 cm, and 0.5 cm respectively. (b) Left, histological analysis of WT and OE leaf cross-sections. Regions outlined in red are shown in greater detail at right. Red arrows indicate bulliform cells (BCs). Scale bars = 200  $\mu$ m and 100  $\mu$ m respectively. (c, d) BC areas (c) and BC numbers (d) in WT and OE leaves. (e–h) Phenotype analysis of *SRL10* knockout (KO) lines. (e) Representative images of 'Nipponbare' (NPB/WT) and *LOC\_Os10g33970* (*SRL10*-KO) mutant whole plants (upper left), leaves (right) and leaf cross-sections (lower left). Scale bars = 20 cm, 2 cm, and 0.5 cm respectively. (f) Left, histological analysis of WT and KO leaf cross-sections. Regions outlined in red are shown in greater detail at right. Red arrows indicate BCs. Scale bars = 200  $\mu$ m and 100  $\mu$ m respectively. (g, h) BC areas (g) and BC numbers (h) in NPB (WT) and *SRL10*-KO (KO) leaves. (i) Subcellular localization of green fluorescent protein (GFP)-*SRL10* fusion protein in rice protoplasts. Scale bar = 5  $\mu$ m. 4',6-diamidino-2-phenylindole (DAPI) staining was used to confirm the nuclear localization. (j) *SRL10* promoter activity in multiple rice tissues as determined by  $\beta$ -glucuronidase (GUS) assays. (k) Relative *SRL10* expression levels in WYJ7 as measured with quantitative reverse transcription PCR (qRT-PCR). Data are given as mean  $\pm$  standard deviation. Asterisks indicate significant difference based on the Student's *t* test: \* for  $P < 0.05$ ; \*\* for  $P < 0.01$ ; ns, not significant.

Surprisingly, CATB, one of the three CAT isoforms that contributes to CAT activity in plants (Matsumura *et al.*, 2002), was shown to interact with *SRL10* (Figure S5). In a domain deletion experiment in yeast, we found that the first dsRBM of *SRL10* interacted weakly with CATB, whereas the second dsRBM showed a strong interaction with CATB (Figure 6a). The interaction between CATB and *SRL10* was further confirmed using several methods: split-luciferase complementation (SLC) (Figure 6b, c), co-immunoprecipitation (Co-IP) (Figure 6d), glutathione S-transferase (GST) pull-down (Figure 6e) and bimolecular

fluorescence complementation (BiFC) assays (Figure S7). The results of all four assays demonstrated that *SRL10* did interact with CATB.

We then disrupted the *CATB* gene in WYJ7 via CRISPR/Cas9 to generate a mutant line, *catb*, containing a 1-bp insertion in the second exon of *CATB* that resulted in early termination of translation (Figure 7a, b, d). *catb* plants exhibited abaxially rolled flag leaves (Figure 7b). A *srl10/catb* double mutant was constructed by crossing *srl10* and *catb*; double mutants had adaxially rolled leaves, similar to those of the *srl10* single mutant. However,

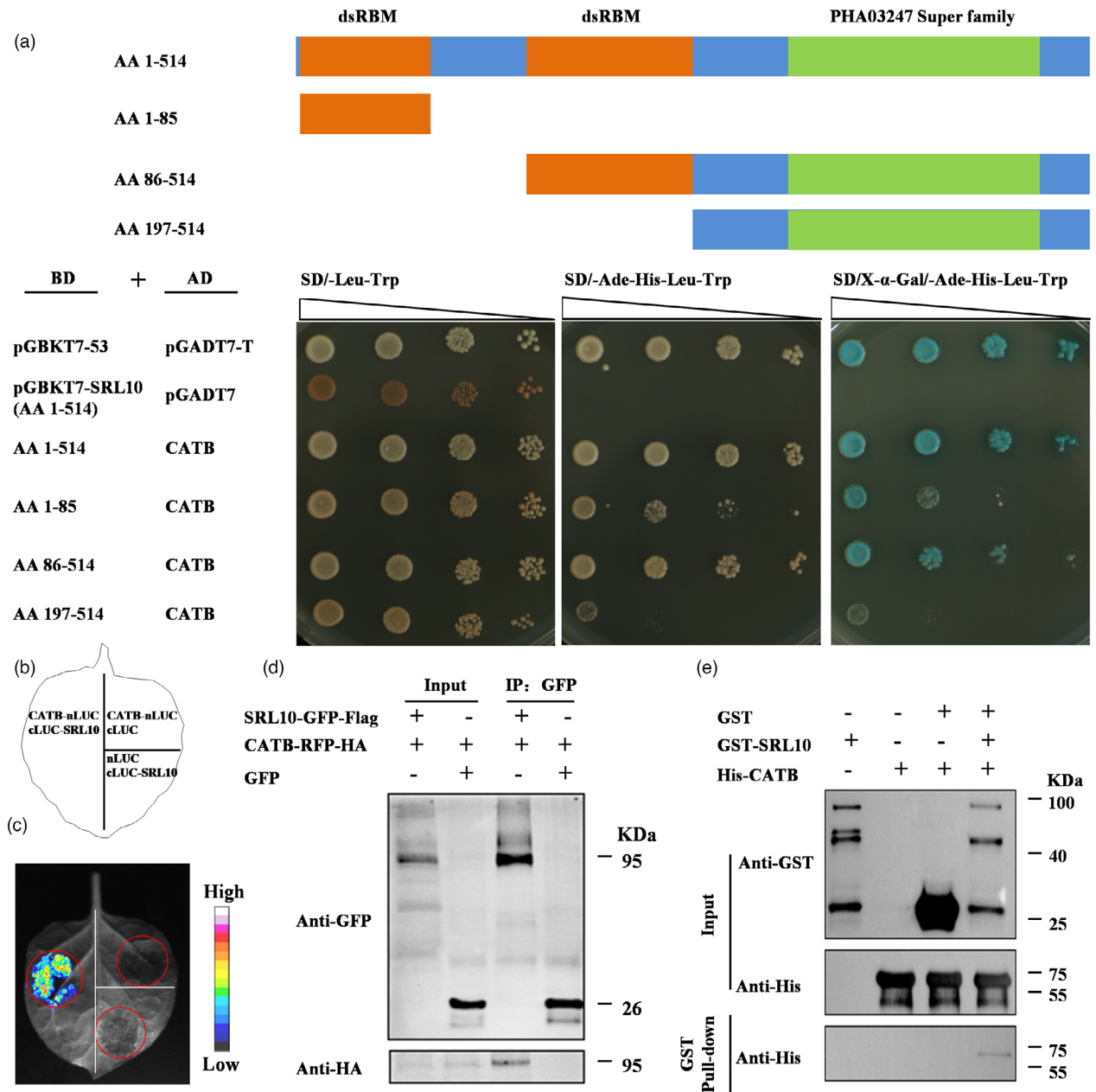


**Figure 6** SRL10 interacts with CATB. (a) Yeast two-hybrid assays showing interactions between SRL10 and CATB. Upper, SRL10 regions tested for interactions with CATB. Lower, co-transformed yeast clones that grew on SD–Leu–Trp medium (left), SD–Leu–Trp–Ade–His medium (middle), and SD–Leu–Trp–Ade–His medium with 0.04 mg·mL<sup>-1</sup> X- $\alpha$ -Galactosidase (right). pGBKT7-53 + pGADT7-T and pGBKT7-SRL10 + pGADT7 were used as the positive and negative controls respectively. (b,c) Interactions between SRL10 and CATB as detected by split-luciferase (SLC) assays in *Nicotiana benthamiana* leaves. Red circles represent injection sites. (d) Co-immunoprecipitation assay. SRL10-GFP-FLAG and CATB-RFP-HA were co-expressed in *N. benthamiana* leaves. Molecular mass markers are shown (kDa). (e) His-CATB, glutathione S-transferase (GST) and GST-SRL10 were purified with pull-down assays and detected with anti-His antibodies (His-CATB) and anti-GST antibodies (GST and GST-SRL10). Molecular mass markers are shown (kDa).

LRI values were lower in the *sr10/catb* double mutant than in *sr10* single mutant plants (Figure 7e). This indicated that knocking out of *CATB* partially masked the *sr10* mutant phenotype, reducing its severity. Further microscopic observation revealed that the BC area was significantly higher in *sr10* and *sr10/catb* mutants than in WYJ7, whereas the mesophyll cell area was significantly less in *sr10* than in WYJ7 and *catb* plants (Figure 7c,f,g).

To clarify the genetic relationship between *SRL10* and *CATB*, we generated a *CATB* overexpression line in the *sr10* background (*pACTIN1::CATB sr10*) and an *SRL10* overexpression line in the *catb* background (*pACTIN1::SRL10 catb*). Overexpression of *CATB* in *sr10* did not reverse the semi-rolled leaf phenotype of *sr10*, and the leaves of *pACTIN1::SRL10 catb* plants were still abaxially curled (Figure 8). These results suggested that both *SRL10* and *CATB* played critical roles in leaf morphogenesis.



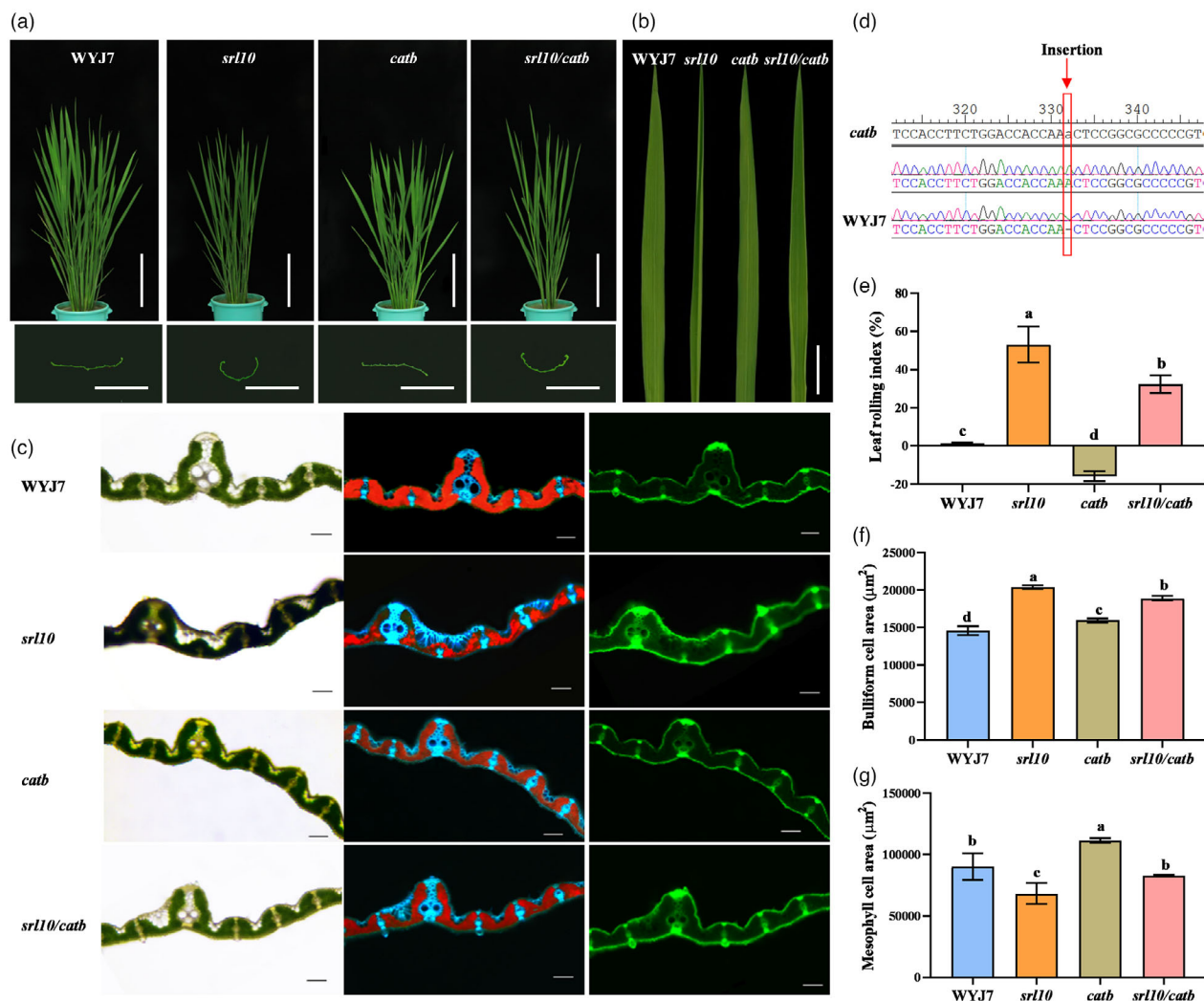


**Figure 7** Mutations of *SRL10* and *CATB* affect the polarity development of rice leaves. (a) Representative whole plants and leaf cross-sections of WYJ7, *srl10*, *catb* and *srl10/catb*. Scale bars = 20 cm and 0.8 cm respectively. (b) Representative leaves of WYJ7, *srl10*, *catb* and *srl10/catb*. Scale bar = 3 cm. (c) Histological analysis of leaf cross-sections in WYJ7, *srl10*, *catb* and *srl10/catb*. Left, visible light. Middle, blue and red fluorescence, with blue indicating vascular bundle sheath, mechanical tissue and phloem, and red indicating mesophyll cells. Right, green fluorescence showing epidermal cells and mechanical tissues. (d) Chromatogram showing sequences of the wild type (WYJ7) and transgenic *CATB* knockout line (*catb*). (e) Leaf rolling index (LRI) values for WYJ7, *srl10*, *catb* and *srl10/catb* plants. (f) Bulliform cell (BC) areas in WYJ7, *srl10*, *catb* and *srl10/catb* plants. (g) Mesophyll cell areas in WYJ7, *srl10*, *catb* and *srl10/catb* plants. Data are shown as mean  $\pm$  standard deviation. Significant differences between groups are marked with different letters (Duncan's multiple range test,  $P < 0.05$ ).

### Overexpression of *SRL10* enhanced thermotolerance in rice via stabilizing *CATB* protein

To verify the role of *SRL10* in thermotolerance, we exposed WYJ7, *srl10* and *SRL10*-overexpression (*OE*) plants to heat stress. Thereafter, we observed the degree of leaf damage and changes of photosynthetic parameters. At 42 °C, *SRL10*-*OE* plants had the smallest reduction in Fv/Fm values and a significantly higher survival rate than WYJ7 and *srl10* (Figure 9d,e). These results suggested that *SRL10*-*OE* plants experienced the least heat-induced photosystem damaged. At these temperatures, *SRL10*-*OE* plants also had the smallest amount of visible damage, whereas *srl10* plants suffered the most damage (Figure 9a,b). These findings were consistent with observed differences in level of H<sub>2</sub>O<sub>2</sub> and malondialdehyde (MDA), a marker of cellular ROS damage, in leaves from each line (Figure 9f,g). This suggested

that although heat stress induced ROS accumulation in all three lines, ROS accumulation was significantly lower in *SRL10*-*OE* than in WYJ7 or *srl10*. In addition, CAT activity was significantly higher in *SRL10*-*OE* than in WYJ7 and *srl10* leaves under heat stress (Figure 9h), consistent with the higher expression levels of *CATB* in *SRL10*-*OE* (Figure 9i,j). These results suggested that overexpression of *SRL10* enhanced CAT activity under heat stress.

Considering that the components in a protein complex may mutually regulate the stability of each unit (Bello *et al.*, 2019), we conducted cell-free degradation assay with His-*CATB* and GST-*SRL10*. The results showed that mixture of GST-*SRL10* and His-*CATB* dramatically elongated the 'half-life' time of the proteins compared to either sample alone in this *in vitro* assay, suggesting that the interaction helped to maintain the stability of each and would promoting normal protein functioning (Figure 9l-o). Increased *CATB* stability due to *SRL10* binding may improve the

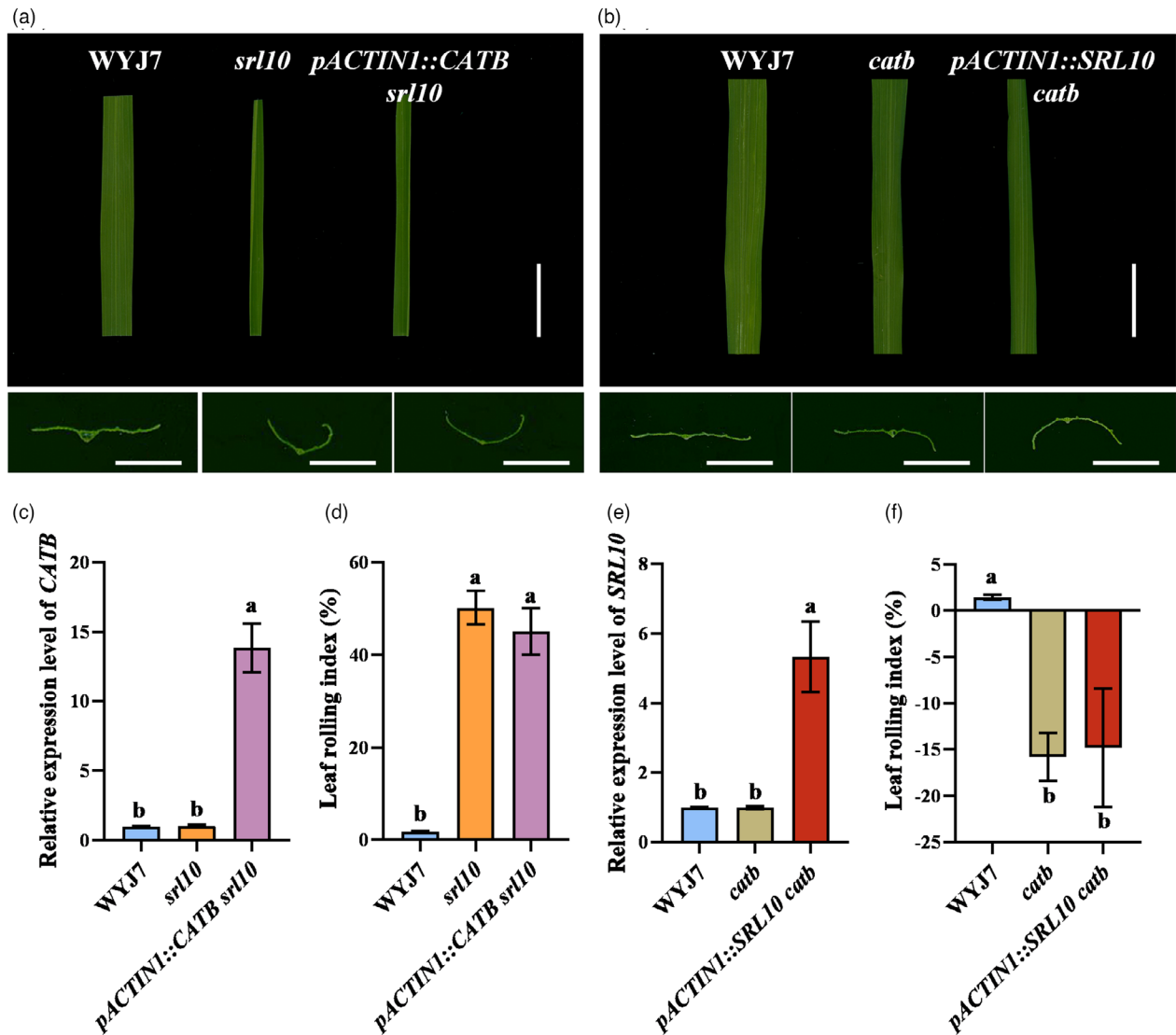


**Figure 8** Complementation analysis of *SRL10* in *catb* mutant and *CATB* in *srl10* mutant. (a) Representative WYJ7, *srl10* and *pACTIN1::CATB srl10* leaves (upper) and leaf cross-sections (lower). Scale bars = 2 cm and 0.3 cm respectively. (b) Representative WYJ7, *catb* and *pACTIN1::SRL10 catb* leaves (upper) and leaf cross-sections (lower). Scale bars = 2 cm and 0.5 cm respectively. (c) Relative expression levels of *CATB* in WYJ7, *srl10* and *pACTIN1::CATB srl10* complementation plants. (d) LRI values for WYJ7, *srl10* and *pACTIN1::CATB srl10* complementation plants. (e) Relative expression levels of *SRL10* in WYJ7, *catb* and *pACTIN1::SRL10 catb* complementation plants. (f) LRI values for WYJ7, *catb* and *pACTIN1::SRL10 catb* complementation plants. Data are shown as mean  $\pm$  standard deviation. Significant differences between groups are marked with different letters (Duncan's multiple range test,  $P < 0.05$ ).

*CATB*-mediated  $H_2O_2$  scavenging ability, and increased *SRL10* stability due to *CATB* binding may be beneficial to plant growth and development processes that are regulated by this DRB protein. Rice is extremely sensitive to heat stress, particularly at the reproductive stage; in this phase, such stress causes declines in seed-setting rate and yield (Xu et al., 2020). We therefore heat-stressed WYJ7, *srl10* and *SRL10-OE* plants at the booting stage. Although heat stress significantly decreased the spikelet fertility in all three lines: the seed-setting rate of *SRL10-OE* plants was still significantly higher than that of WYJ7 and *srl10* plants (by 2.41 times and 6.02 times respectively) at 42 °C (Figure 9c,k). Taken together, these results implied that *SRL10* positively regulated rice thermotolerance by enhancing *CAT* activity and stabilizing *CATB*.

### Haplotype analysis of *SRL10*

The results discussed above demonstrated a crucial role of *SRL10* in rice leaf morphology and thermotolerance, we therefore performed haplotype analysis on 3025 rice accessions to identify alleles. We identified three single nucleotide polymorphisms (SNPs) within the *SRL10* coding sequence (CDS): SNP1<sup>AG</sup> (18105284), SNP2<sup>AG</sup> (18104024) and SNP3<sup>CT</sup> (18103611) (Figure 10a). Based on these three SNPs, the rice accessions could be grouped into three main haplotypes: Hap1 (AAC), Hap2 (GGT) and Hap3 (AGC). *Japonica* rice almost exclusively carried Hap1 (AAC), *indica* rice carried both Hap2 (GGT) and Hap3 (AGC) and *aus* rice primarily carried Hap3 (AGC) (Figure 10b).

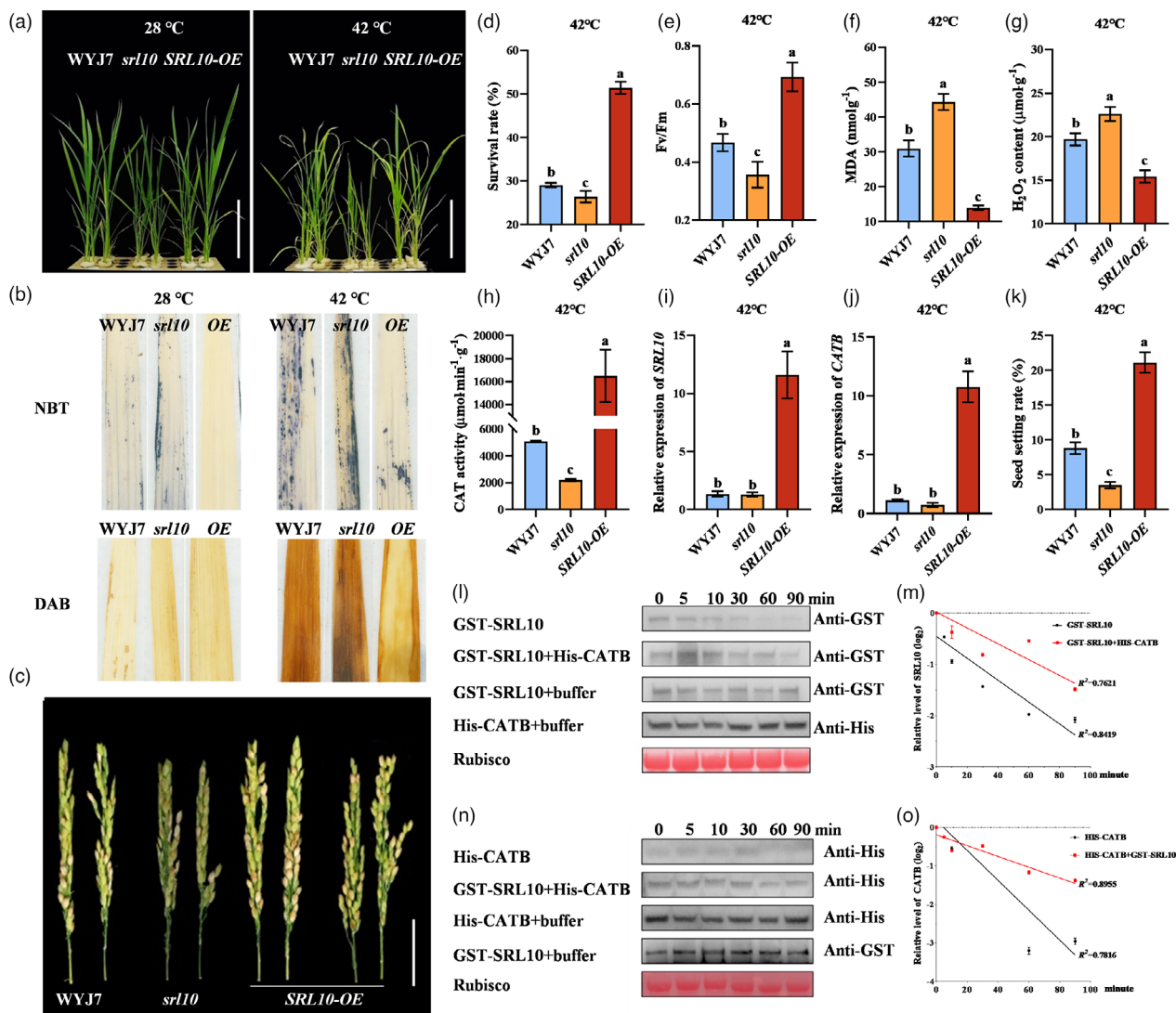


**Figure 9** Overexpression of *SRL10* enhances thermotolerance in rice. (a) Representative images of WYJ7, *srl10* and *SRL10*-overexpression (*OE*) plants grown at 28 °C or 42 °C for 48 h. Scale bar = 10 cm. (b) Nitroblue tetrazolium (NBT) and 3, 3'-diaminobenzidine (DAB) staining in WYJ7, *srl10* and *SRL10*-*OE* plants grown at 28 °C or 42 °C for 48 h. (c) Spike morphology of WYJ7, *srl10* and *SRL10*-*OE* plants at booting stage. (d) Survival rates of WYJ7, *srl10* and *SRL10*-*OE* plants grown at 42 °C for 7 days. (e)  $F_v/F_m$  measurements of WYJ7, *srl10* and *SRL10*-*OE* plants grown at 42 °C for 48 h. (f–h) Malondialdehyde (MDA) content (f),  $H_2O_2$  levels (g) and catalase activity (h) in leaves of WYJ7, *srl10* and *SRL10*-*OE* plants grown at 42 °C for 48 h. (i,j) Relative expression level of *SRL10* (i) and *CATB* (j) in leaves of WYJ7, *srl10* and *SRL10*-*OE* plants grown at 42 °C for 48 h. (k) Seed setting rates of WYJ7, *srl10* and *SRL10*-*OE* plants in the booting stage after growth at 42 °C for 7 days. (l,m) Degradation assay (l) and degradation curve (m) of glutathione S-transferase (GST)-tagged *SRL10* in the absence or presence of His-tagged *CATB*. Equal starting amounts of total protein were used for the degradation reactions, as indicated by Ponceau S staining. (n,o) Degradation assay (n) and degradation curve (o) of His-*CATB* in the absence or presence of GST-*SRL10*. Equal starting amounts of total protein were used for each degradation reaction as indicated with Ponceau S staining. Data are shown as mean  $\pm$  standard deviation. Significant differences between groups are marked with different letters (Duncan's multiple range test,  $P < 0.05$ ).

### Natural variations of *SRL10* were associated with field thermotolerance in rice

We next carried out a series of experiments to clarify whether the haplotypes that we identified conferred varying levels of thermotolerance in rice. Heading dates were recorded for plants with different haplotypes (Table S6). Meteorological data from the summer of 2020 and 2021 in the Fuyang district of Hangzhou (Figure 10c), where the rice plants were grown, showed that plants experienced higher temperature at the booting stage of these accessions in 2020 than in 2021. The

temperature difference between 2020 and 2021 led to difference in yield-trait performance between 2 years; the seed-setting rate and grain yield per plants with Hap3 (AGC) were significantly higher than those with Hap1 (AAC) (Figure 10d–g). This suggested that Hap3 (AGC) contributed to subspecies-specific heat resistance.

We next applied heat stress (42 °C) to rice accessions with each of the three haplotypes at the booting stage in growth chamber conditions. Although spikelet fertility was significantly decreased in plants with all three haplotypes at 42 °C, seed-setting rate was significantly higher for plants carrying Hap3 (AGC) allele than for

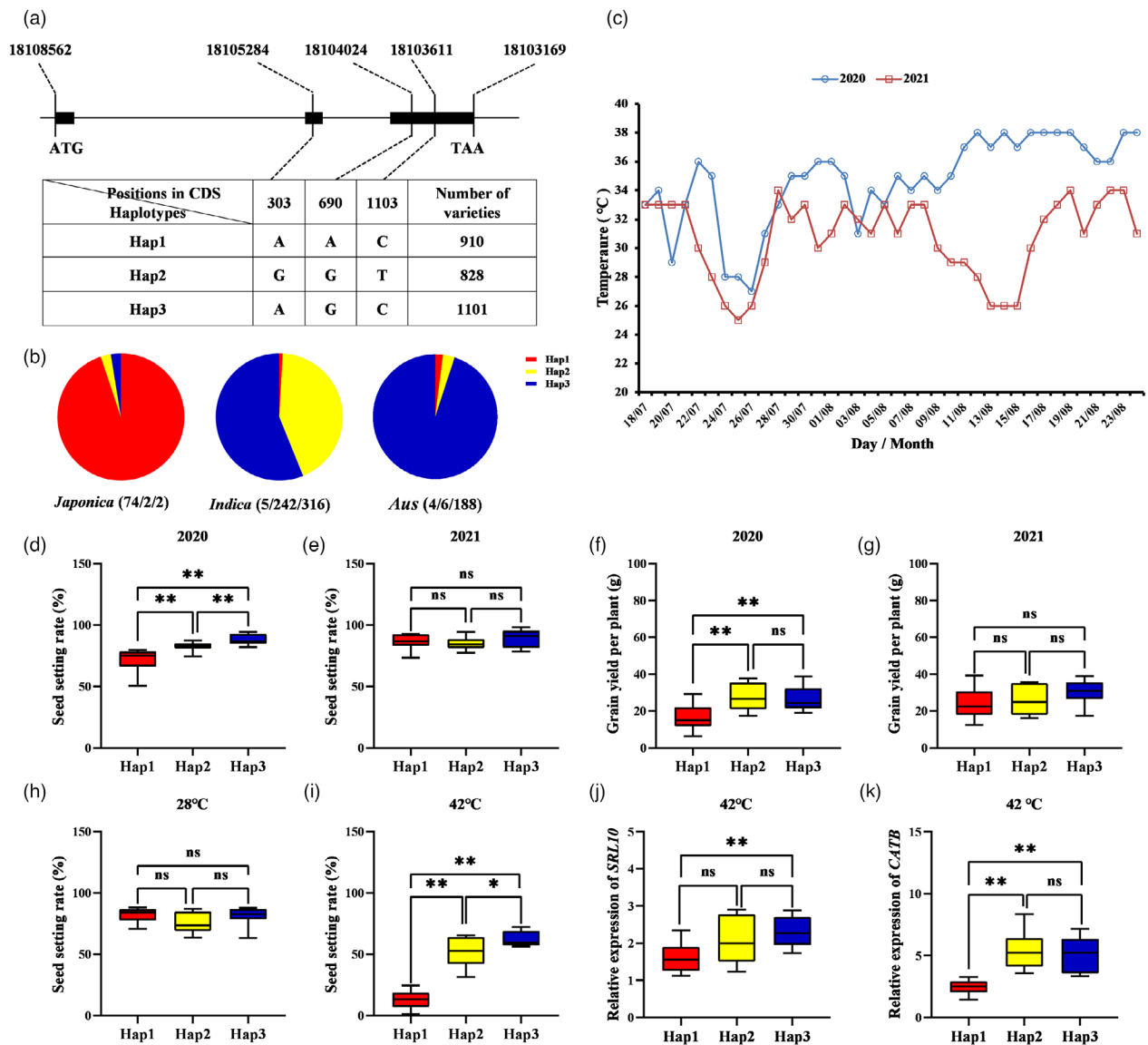


**Figure 10** Natural variations in *SRL10* were associated with thermotolerance. (a) Three major haplotypes (Hap1–3) in the *SRL10* coding region. (b) Distribution of Hap1–3 in three rice subgroups: *japonica*, *indica* and *aus*. Hap1, Hap2 and Hap3 are indicated with red, yellow and blue respectively. The number of accessions with each haplotype is shown in brackets (*japonica/indica/aus*). (c) Temperature changes in Fuyang District over 1 month during the reproductive growth stage in 2020 and 2021. (d,e) Statistical analysis of the seed-setting rate of accessions carrying Hap1–3 in 2020 (d) and 2021 (e). (f,g) Statistical analysis of grain yield per plant for accessions carrying Hap1–3 in 2020 (f) and 2021 (g). (h,i) Seed-setting rates of accessions carrying Hap1–3 after growth at 28 °C (h) or 42 °C (i) for 3 days at the booting stage. (j,k) Relative expression of *SRL10* (j) and *CATB* (k) in accessions carrying Hap1–3 after growth at 42 °C for 48 h in the seedling stage. Data are given as mean  $\pm$  standard deviation. Asterisks indicate significant difference based on the Student's *t* test: \* for  $P < 0.05$ ; \*\* for  $P < 0.01$ ; ns, not significant.

those carrying Hap1 (AAC) or Hap2 (GGT) allele (4.92 times and 1.21 times higher respectively) (Figure 10h,i). Moreover, the relative expression levels of *SRL10* and *CATB* were significantly higher in plants carrying Hap3 (AGC) allele than those carrying Hap1 (AAC) allele at 42 °C (Figure 10j,k).

Subsequently, we selected the near-isogenic lines (NILs) NIL-*SRL10*<sup>Hap1</sup> and NIL-*SRL10*<sup>Hap3</sup>, which carried Hap1 (AAC) and Hap3 (AGC) genotypes respectively. Under field conditions, NIL-*SRL10*<sup>Hap1</sup> plants had significantly lower seed-setting rate and grain number per plant compared to NIL-*SRL10*<sup>Hap3</sup> plants (Figure 11a–d). Furthermore, for plants grown in a growth chamber at 42 °C, the seed-setting rate and grain yield per plant

were significantly higher in NIL-*SRL10*<sup>Hap3</sup> plants than in NIL-*SRL10*<sup>Hap1</sup> plants (3.18 times and 1.68 times higher respectively) (Figure 11e–i). Under heat stress, *SRL10* and *CATB* were also expressed at lower levels in NIL-*SRL10*<sup>Hap1</sup> than NIL-*SRL10*<sup>Hap3</sup> plants at the seedling stage (Figure 11j,k). More importantly, *SRL10* was more stable at 42 °C in NIL-*SRL10*<sup>Hap3</sup> than in NIL-*SRL10*<sup>Hap1</sup> plants after 30 min of heat exposure (Figure 11l,m). These results suggested that Hap3 (AGC) type of the *SRL10* allele, which was present in the majority of *aus* rice cultivars, was highly associated with subspecies-specific heat resistance; this demonstrated the important role of *SRL10* in rice thermotolerance in nature.



## Discussion

### SRL10 determines leaf morphology by regulating the development of bulliform cells

In this study, we identified *SRL10* as a key regulator of leaf rolling through knockout and overexpression analysis. Compared to wild type, the knockout line of *SRL10* had higher numbers and size of BCs, leading to adaxial leaf rolling. In contrast, overexpression of *SRL10* led to decreased BC number and area, which resulted in abaxial leaf rolling. Our data therefore strongly support a negative role of *SRL10* in the formation and development of BCs on adaxially leaf surface. Besides, *SRL10* might also regulate sclerenchyma cell development; the disappearance of sclerenchyma cells on the adaxial surface caused BCs on both sides of the small vascular bundle to connect in *srl10* and *SRL10-KO* plants. BCs are highly linked to rolled leaf phenotype in rice (Xu *et al.*, 2018; Zhang *et al.*, 2015b) and defective development of BC in particular is responsible for the rolled leaf phenotype of many mutants (Zhou *et al.*, 2018). We therefore hypothesized that adaxially rolled leaves in *srl10* were primarily a result of changes in the number and area of BCs. Many genes that contribute to BC development have been identified, such as *LATERAL ORGAN BOUNDARIES DOMAIN (LBD)* gene *OsLBD3-7* (Li *et al.*, 2016a), *ROP-INTERACTING RECEPTOR-LIKE KINASE 1 (OsRRK1)* (Ma *et al.*, 2017) and *LEAF ROLLING RECEPTOR-LIKE CYTOPLASMIC KINASE 1 (LRRK1)* (Zhou *et al.*, 2018). Thus, the identification and cloning of *SRL10* conducted in the present study expands the known molecular regulatory network of leaf morphological development in rice.

### SRL10 regulates both leaf morphology and thermotolerance in rice

Transcriptomic analysis and qRT-PCR showed that DEGs related to leaf development between WYJ7 and *srl10* were primarily enriched in phytohormone signal transduction pathways, including *OsCOW1* and *RL14* (Figure S1a–c). *OsCOW1* encodes a member of the YUCCA protein family and affects water homeostasis in rice (Woo *et al.*, 2007). *RL14* modulates leaf rolling by affecting water transport in leaves (Fang *et al.*, 2012). Moreover, miR165/miR166 have prominent roles in abaxial leaf fate by targeting the HD-ZIP III genes *PHB*, *REV* and *PHV* (Fouracre & Poethig, 2016; Nogueira *et al.*, 2007; Sakaguchi & Watanabe, 2012; Zhang *et al.*, 2018). The HD-ZIP genes *OSHB1/LF1* and *OSHB4* regulate leaf development in an auxin-dependent manner in rice (Li *et al.*, 2016b; Zhang *et al.*, 2021b). Therefore, the differential expression of miR166m and its target genes (*OSHB1*, *OSHB2*, *OSHB4*, *YABBY5*) in WYJ7 and *srl10* indicated that *SRL10* affects leaf polarity by participating in complex regulatory network involving auxin, miRNA and transcription factors.

Numerous studies have demonstrated that *CATB* functions as a key H<sub>2</sub>O<sub>2</sub> scavenging enzyme (Ye *et al.*, 2011; Zhang *et al.*, 2016), but its role in leaf morphology has rarely been reported. In the present study, loss of *CATB* function was found to result in abaxially rolled flag leaves and up-regulation of miR399 acumination (Figure S6b). In contrast, the *srl10/catb* double mutant exhibited adaxially rolled leaves, suggesting that *CATB* did control leaf morphology. *Arabidopsis CATALASE2* have been reported to influence leaf morphology by changes of auxin levels (Gao *et al.*, 2014). Notably, auxin can induce the production of ROS, in turn, ROS downstream product reactive carbonyl species (RCS) regulates auxin signal transduction in a

feed-forward manner (Biswas *et al.*, 2019). Therefore, the complex crosstalk between auxin and H<sub>2</sub>O<sub>2</sub> could be a reasonable explanation for the regulatory function of *CATB* on leaf morphology (Biswas *et al.*, 2019; Li *et al.*, 2021). However, the regulatory relationship between H<sub>2</sub>O<sub>2</sub> and auxin in *catb* plants requires further investigation. We speculated that the loss of *CATB* function might result in changes of auxin level *in vivo*, thereby leading to changes in histocytes and rolled leaf in rice. In this study, the regulatory role of *SRL10* on rolled leaf might be related to the development of bulliform cells regulated by miRNA-auxin. Moreover, the interaction between *SRL10* and *CATB* may further affect the crosstalk between H<sub>2</sub>O<sub>2</sub> and auxin. Collectively, we speculated that the crosstalk of *SRL10*-miRNA-auxin and H<sub>2</sub>O<sub>2</sub>-auxin jointly regulates the balance of auxin metabolism *in vivo*, endowing *SRL10* with synergistic effect on leaf morphology and stress resistance.

ABA regulates stress resistance through modulation of stomatal aperture and leaf transpiration capacity (Li *et al.*, 2020). We here found that *SRL10* participates in heat stress response and ABA response. Furthermore, H<sub>2</sub>O<sub>2</sub> is a critical signalling molecule in plants, and the balance between H<sub>2</sub>O<sub>2</sub> generation and scavenging rates contributes to normal plant development and stress resistance (Zhang *et al.*, 2016). Although CAT is the primary enzyme responsible for scavenging H<sub>2</sub>O<sub>2</sub>, its affinity for H<sub>2</sub>O<sub>2</sub> is extremely low (Foyer *et al.*, 2009; Mhamdi *et al.*, 2012; Zhang *et al.*, 2016). The substrate channelling mechanism used in processes such as ROS scavenging suggested that binding of enzymes to other substances can greatly accelerate the reaction rate (Singleton *et al.*, 2014; Zhang, 2011; Zhang *et al.*, 2016). Thus, interaction between *SRL10* and *CATB* may affect the affinity of CAT for H<sub>2</sub>O<sub>2</sub>, altering its H<sub>2</sub>O<sub>2</sub> scavenging capacity. We observed significantly higher CAT activity and *CATB* expression levels in the leaves of *SRL10-OE* plants, which led to lower H<sub>2</sub>O<sub>2</sub> levels. This suggested that overexpression of *SRL10* enhanced CAT activity under heat stress. Moreover, *SRL10*-*CATB* interactions contributed to the stability of both proteins. We therefore speculate that *SRL10* participates in H<sub>2</sub>O<sub>2</sub> metabolism, positively regulating thermotolerance by interacting with and stabilizing *CATB*.

The role of *SRL10* in regulating thermotolerance may also be related to complex miRNA-mediated regulatory networks. In *Arabidopsis*, *AtDRB2* is required for appropriate regulation of the miRNA399/PHOSPHATE2 expression module (Pegler *et al.*, 2019), which alters the salt stress response (Pegler *et al.*, 2020). This suggests that differential expression of miR399 in WYJ7 and *srl10* may also be related to thermotolerance. Furthermore, high temperature-triggered increase in transpiration rate was considered as a strategy of enabling 'heat avoidance' by lowering leaf temperature (Aparecido *et al.*, 2020; Haddad *et al.*, 2021; Lin *et al.*, 2017; Crawford *et al.*, 2012). The complex relationships between cell wall structure, stomatal morphology, leaf water balance and the transpiration rate could underlie *srl10* sensitivity to high temperature. The role of *SRL10* in controlling thermotolerance appears to be complex and regulated by miRNA, ROS metabolism and other unknown factors. The details of these regulatory mechanisms are not yet clear, demonstrating a need for further in-depth research in the future. Identifying new regulatory genes downstream of *SRL10* should be focus of subsequent studies; this would further clarify the role of *SRL10* in leaf morphology and thermotolerance. Our results serve as a reference for gene discovery and simultaneous molecular breeding of rice thermotolerance and leaf morphology.

### SRL10 has pleiotropic effects on rice growth and development

Most dsRBM-containing proteins have a second functional or catalytic domain, suggesting that such proteins participate in

multiple biological processes such as miRNA biosynthesis (Burd and Dreyfuss, 1994), abiotic stress responses (Raghuram et al., 2015) and hormone signalling (Lu and Fedoroff, 2000). SRL10 contains two dsRBMs and a putative PHA03247 superfamily UL36 domain. We here found that a C to T substitution in

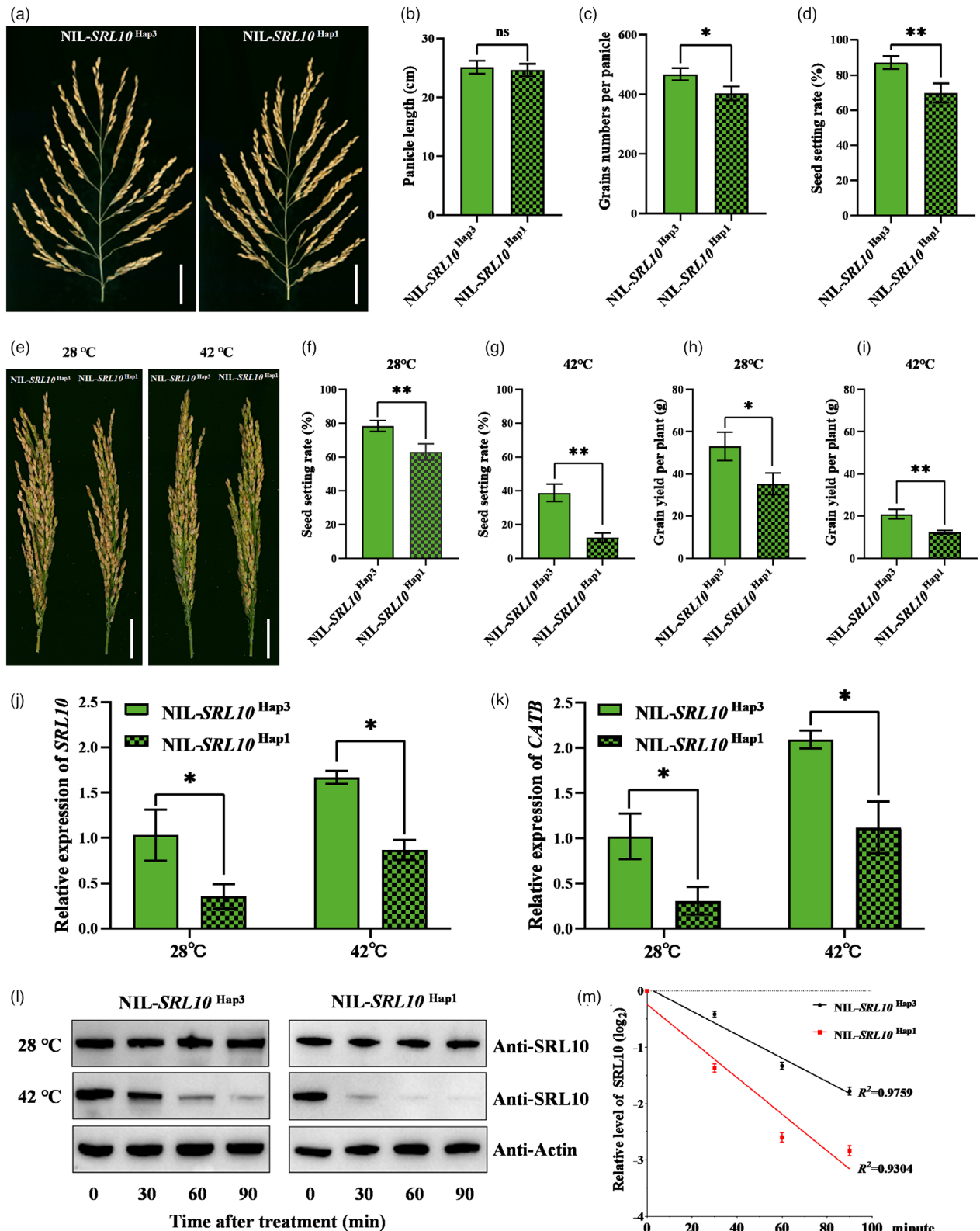


**Figure 11** Analysis of thermotolerance in NIL-*SRL10*<sup>Hap3</sup> and NIL-*SRL10*<sup>Hap1</sup> plants. (a) Comparison of panicles from the near-isogenic lines (NILs) NIL-*SRL10*<sup>Hap3</sup> and NIL-*SRL10*<sup>Hap1</sup>. Scale bar = 3 cm. (b–d) Panicle length (b), grain numbers per panicle (c) and seed-setting rate (d) of NIL-*SRL10*<sup>Hap3</sup> and NIL-*SRL10*<sup>Hap1</sup>. (e) Spike morphology of NIL-*SRL10*<sup>Hap3</sup> and NIL-*SRL10*<sup>Hap1</sup> plants grown at 28 °C or 42 °C for 3 days at the booting stage. (f,g) Seed-setting rate of NIL-*SRL10*<sup>Hap3</sup> and NIL-*SRL10*<sup>Hap1</sup> plants grown at 28 °C (f) or 42 °C (g) for 3 days at the booting stage. (h–i) Grain yield per plant of NIL-*SRL10*<sup>Hap3</sup> and NIL-*SRL10*<sup>Hap1</sup> plants grown at 28 °C (h) or 42 °C (i) for 3 days at the booting stage. (j–k) Relative expression levels of *SRL10* (j) and *CATB* (k) in NIL-*SRL10*<sup>Hap3</sup> and NIL-*SRL10*<sup>Hap1</sup> plants grown at 28 °C or 42 °C for 48 h at the seedling stage. (l) Thermal stability analysis of SRL10 *in vivo*. Protein abundance was visualized via immune detection with anti-SRL10 antibodies. Equal protein loading was confirmed with anti-actin antibodies. (m) Degradation curve of SRL10 in NIL-*SRL10*<sup>Hap3</sup> and NIL-*SRL10*<sup>Hap1</sup> plants grown at 42 °C. Data are given as mean ± standard deviation. Asterisks indicate significant difference based on the Student's *t* test: \* for *P* < 0.05; \*\* for *P* < 0.01; ns, not significant.

the first exon of *SRL10* led to an amino acid change in the first dsRBMs of SRL10 and was associated with the adaxial leaf rolling phenotype in *srl10*. A complementation assay showed that expression of *LOC\_Os10g33970* in *srl10* rescued the semi-rolled leaf and temperature-sensitive phenotypes.

Interaction between SRL10 and CATB were verified both *in vitro* and *in vivo* with Y2H, Co-IP, SLC, GST pull-down and BiFC assays. We also confirmed that CATB-GFP was localized to the peroxisome (Figure S7). In addition, we repeated the BiFC assay confirming the interaction between CATB and SRL10 with multiple organelle-specific fluorescent markers (such as peroxisomes, ER, mitochondria and Golgi apparatus) and strong yellow fluorescent protein (YFP) signal was consistently observed, indicating interactions between SRL10 and CATB. However, there was no overlap observed between the YFP signal and any of the organellar markers. This might have been due to the complexity of protein expression (Tanz *et al.*, 2013) or an unknown interaction mechanism. For example, some active proteins exist in multiple organelles and are shuttled between five or six subcellular structures (Carrie and Small, 2012; Small *et al.*, 1998). Gao *et al.* (2021) found that co-expression of ROD1 and CATB changed the localization of CATB. The details of interactions between CATB and SRL10 therefore require further investigation.

Most of the known proteins identified as SRL10 interactors here participate in multiple biological processes. For example, rice snf1-related protein kinase 1 (SnRK1) family members SnRK1A mediates glucose metabolism (Lu *et al.*, 2007); VASCULAR PLANT ONE-ZINC FINGER 1 (VOZ1) mediates immune response (Wang *et al.*, 2021a); and AUTHENTIC HIS PHOSPHOTRANSFER PROTEIN 2 (AHP2) mediates drought and salt resistance (Figure S5) (Sun *et al.*, 2014). Moreover, the loss of *SRL10* function resulted in open glumes, imperfect grain filling and reduced 1000-grain weight. We therefore hypothesize that *SRL10* has pleiotropic functions, including regulation of plant growth and resistance to environmental stresses.

### Prospects for applying *SRL10* in rice molecular breeding for stress resistance and high yield

Ideal plant architecture and strong stress tolerance are the two major targets of high-yield breeding. Although many high temperature-tolerant germplasm resources have been identified, few varieties have strong thermotolerance without associated yield decreases. We here confirmed that natural variation of *SRL10* associated with field thermotolerance by analysing yield-trait performance and SRL10 thermal stability in accessions with different *SRL10* haplotypes (NIL-*SRL10*<sup>Hap1</sup> and NIL-*SRL10*<sup>Hap3</sup>) under heat stress (42 °C). These results suggested that advantages in heat resistance were conferred by Hap3 (AGC) type of *SRL10* allele, which resulted from higher *SRL10* expression levels and protein stability; this minimized heat-induced plant damage

without decreasing yield. Because elite rice varieties containing Hap3 (AGC) exhibit stronger thermotolerance without an obvious decline in productivity, this natural variation of *SRL10* constitutes an elite allelic variation for high-yield breeding through ideal plant architecture and high thermotolerance. Collectively, our combined analysis of leaf morphology and thermotolerance revealed that integration of favourable *SRL10* alleles could accelerate inter-regional exchange of high-performance rice germplasm resources, thus promoting sustainable development in global agriculture.

## Materials and methods

### Plant materials and growth conditions

*Oryza sativa* ssp. *japonica* variety WYJ7 seeds were mutagenized with a 1% EMS solution. Rice plants were grown in experimental fields at the China National Rice Research Institute in Fuyang District (Zhejiang Province, China) (30°4'52" E, 119°55'54" N) under natural environmental conditions. A forward genetic screen was then conducted for high temperature sensitivity and altered leaf morphology.

To test heat tolerance, seedlings were grown in growth chambers under control temperature conditions (28 °C/25 °C day/night temperature) or heat stress condition (42/25 °C day/night temperature) at the three-leaf and five-leaf stages. Plants were cultured in nutrient soil and hydroponic media, respectively, at 70%–80% relative humidity with a 14/10 h light/dark period. Seedlings cultured in hydroponic media were also treated with 50 μm ABA for 12 h at the five-leaf stage.

For heat stress treatment, seedlings were cultured in paddy soil under a natural environment. At the booting stage, rice plants were divided into two groups and moved into separate plant growth chambers. One group of rice plants was grown under heat stress condition (42 °C from 10:00 to 16:00/28 °C from 16:01 to 9:59 for 3 or 7 days). The other group served as the control (28 °C from 10:00 to 16:00/25 °C from 16:01 to 9:59 for 3 or 7 days). Both groups were maintained with 70%–80% relative humidity and 800 μmol · m<sup>-2</sup> · s<sup>-1</sup> of light.

### Map-based cloning

To map the *SRL10* locus, an F<sub>2</sub> population derived from a cross between *srl10* and TN1 and newly developed simple sequence repeat (SSR) or sequence-tagged site (STS) markers were used (Table S2). To identify the mutation site, genomic DNA fragments of candidate genes were amplified (Table S3) from WYJ7 and *srl10*, sequenced, and compared using SeqMAN (DNASTAR).

### Constructs for transgenic plants

To construct the genomic DNA complementation vector, the 8796-bp *SRL10* genomic DNA sequence (including 2109-bp

upstream of the start codon, 5394-bp coding region of *SRL10* and 1293-bp downstream of the stop codon) was amplified from WYJ7 and was cloned into the binary vector *pCAMBIA1300*. To construct the *SRL10* and *CATB* CRISPR/Cas9 vectors, the target sequences of single guide RNAs (sgRNAs) were designed and then the OsU3-*SRL10* and OsU3-*CATB* sgRNA expression cassettes were assembled in *pYLCRISPR/Cas9-MH* (Ma *et al.*, 2015). To construct the overexpression vector (*pUbi::attR-SRL10-GFP-3 × FLAG*) of *SRL10*, the full-length coding sequence of *SRL10* was amplified from Nipponbare, then firstly cloned into the *pDONR ZEO* (Invitrogen), and recombined into the *pUbi::attR-GFP-3 × FLAG*. To generate *pACTIN1::SRL10 catb* and *pACTIN1::CATB srl10* complementation lines, the full-length coding region of *SRL10* or *CATB* was inserted into the *pCAMBIA2300-ACTIN1* vector. All resulting constructs were transformed into rice calli via *Agrobacterium tumefaciens*-mediated transformation (Toki *et al.*, 2006). All the primers used in plasmid construction are shown in Table S4, and all of the constructs were confirmed by sequencing.

### Phylogenetic analysis

Protein sequences of *SRL10* were obtained from Rice Genome Annotation Project (<http://rice.uga.edu/index.shtml>). The sequences used in the phylogenetic analysis were obtained by a BLASTP search using the amino acid sequence of *SRL10* as the query at the National Center for Biotechnology Information (NCBI, <http://www.ncbi.nlm.nih.gov/>). Multiple sequence alignments of protein were done using the DNAMAN program. A phylogenetic tree of aligned sequence was constructed in MEGA software with the bootstrap method and 1000 replicates (Gao *et al.*, 2021; Qiu *et al.*, 2018).

### Histological promoter-GUS assay

To construct the *SRL10* promoter-driven GUS reporter gene, a 2109-bp fragment upstream of the *SRL10* start codon (Table S4) was amplified and cloned into the *EcoRI* and *NcoI* sites of the binary vector *pCAMBIA1305.1*. The recombinant vector was then introduced into WYJ7 calli to generate transgenic plants. Several tissues from *SRL10<sub>promoter</sub>::GUS* transgenic rice was stained for GUS activity as previously described (Jefferson *et al.*, 1987).

### Subcellular localization of *SRL10*

For detection of the subcellular localization of *SRL10*, the full-length cDNA of *SRL10* amplified (primers used are listed in Table S4) from Nipponbare rice was cloned into the pBeacon-NeGFP vector using the Gateway cloning system (Invitrogen). The result construct GFP-*SRL10* was transformed into rice protoplasts by the polyethylene glycol (PEG)-mediated transformation method (Yu *et al.*, 2014). Green fluorescent protein (GFP) signals were observed by laser scanning confocal microscopy (Zeiss LSM 700).

### Measurement of physiological indices

The leaf rolling index (LRI) of rice plants was measured according to the method described by Xiang *et al.* (2012). The distance of leaf blade margins in the natural state ( $L_n$ ) and in the unfolding state ( $L_w$ ) in different lines was measured. LRI was then calculated with the following formula:  $LRI (\%) = (L_w - L_n) \times 100 / L_w$ . Fresh leaves of WYJ7 and *srl10* were weighed at specified times to determine the water loss rate of detached blade. Leaf water content was determined as described previously (Qiu *et al.*, 2019).

### ROS-related measurements

CAT activity,  $H_2O_2$  and MDA content were quantified in leaves grown under heat stress for 48 h according to the manufacturer's instructions by using corresponding kits from Geruisi (<http://www.geruisi-bio.com/>). Nitro blue tetrazolium (NBT) staining and 3, 3'-diaminobenzidine (DAB) staining were performed as previously described (Thordal-Christensen *et al.*, 1997).

### Histology and microscopic observations

For freehand section, the leaves were sliced into thin slice by a double blade, and then were observed and photographed using a fluorescence microscope (Leica DM4 B). Paraffin section analysis was performed by using the middle part of each leaf at seedling stage as previously described by Ruan *et al.* (2020). For frozen cross-section assays, the leaves were immersed in the frozen embedding agent (Tissue-Tek® O.C.T. Compound, SAKURA, JAPAN) for 2–3 h at  $-20^\circ C$ . Sections (15  $\mu m$ ) were cut with a freezing microtome (Leica CM1950). Slices were observed and photographed using a microscope (Leica DM4 B). Cellulose, hemicellulose, and pectin levels were measured in WYJ7 and *srl10* according to Zhong and Läuchli (1993). The youngest fully expanded leaves of the rice plants were used for analysis of stomatal index and cell wall as described previously (Zhang *et al.*, 2021). The areas of BCs, number of stomata, and stomatal aperture were calculated using Image J software (Ma *et al.*, 2017).

### Measurement of photosynthetic parameters

The photosynthetic parameters of WYJ7 and *srl10* were measured at the tillering stage with a Li-COR 6400 portable system according to the method described by Li *et al.* (2020).

### Determination of agronomic traits

Agronomic traits such as effective panicle number, numbers of branches, grain numbers per panicle, seed-setting rate, grain yield per plant and 1000-grain weight were measured at the mature stage. To measure the grain filling rate, representative samples from the main panicle at 3, 6, 9, 12, 15, 19, 21, 24 and 27 d after flowering were used to measure the dry weight.

### RNA extraction and quantitative real-time PCR

Total RNA was extracted using the Total RNA Miniprep kit (Axygen, China) according to the manufacturer's instruction. First-strand cDNA and the miRNA first-strand cDNA were synthesized using the ReverTra Ace qPCR-RT kit (Toyobo, Japan) and miRNA 1st Strand cDNA Synthesis Kit (by stem-loop) (Vazyme, <https://www.vazyme.com/Home.html>) according to the user's manual respectively. Quantitative real-time PCR (qRT-PCR) analyses were performed using SYBR Premix Ex Taq (Takara, Japan) and gene-specific primers (Table S5) on a CFX96TM Real-Time System with snRNA U6 or *Ubiquitin (UBQ)* as an internal control.

### Yeast two-hybrid assays

In yeast two-hybrid (Y2H) assays, for DNA-binding domain (BD)-fused *SRL10*, the full-length coding sequences of *SRL10* (Table S4) were fused in-frame to the GAL4 BD in the *pGBKT7* bait vector. For activation domain (AD)-fused *CATB*, the full-length coding sequences of *CATB* (Table S4) were fused in-frame to the GAL4 AD in the *pGADT7* prey vector. For a domain deletion experiment, we divided the full-length coding sequences of *SRL10* into



three segments and they were cloned into *pGBK77* respectively. Different combinations of bait and prey constructs were co-transformed into the yeast strain Y2H Gold as described previously (Ruan *et al.*, 2020).

### Bimolecular fluorescence complementation assay

The cDNA of *SRL10* was cloned into *pSAT1A-cEYFP-N1 (pE3080)* for C-terminal fusion and the cDNA of *CATB* was cloned into *pSAT1A-nEYFP-N1 (pE3079)* for N-terminal fusion (primers used are listed in Table S4). YN + YC-SRL10 and YN-CATB + YC served as controls. YN-CATB and YC-SRL10 were then co-transformed pair-wise into protoplasts by PEG-mediated transformation (Yu *et al.*, 2014).

### Split-luciferase complementation assay

The coding sequences of *CATB* and *SRL10* (Table S4) were inserted into the N-terminal (nLUC) and C-terminal (cLUC) portions of firefly luciferase (LUC) respectively. Split-luciferase complementation assay were performed according to the method described previously (Liang and Li, 2022) by using the resulting plasmids nLUC-CATB and cLUC-SRL10.

### Co-immunoprecipitation assays

The full-length coding sequences of *SRL10* and *CATB* (Table S4) were cloned into the *pCAMBIA1300-Ubi::GFP-3 × FLAG* vector and *pCAMBIA1300-Ubi::RFP-HA* vector respectively. *pCAMBIA1300-Ubi::CATB-RFP-HA* was transiently co-expressed with empty *pCAMBIA1300-Ubi::GFP-3 × FLAG* or *pCAMBIA1300-Ubi::SRL10-GFP-3 × FLAG* in *N. benthamiana*. The detailed co-immunoprecipitation assays were performed as previously described (Wang *et al.*, 2020b).

### Pull-down assay

The coding sequence of *SRL10* and *CATB* was cloned into *pGEX-4 T-1* and *pET28a* respectively (primers used are listed in Table S4). The GST-SRL10 fusion construct was transformed into *Escherichia coli* BL21 (DE3), and the recombinant protein GST-SRL10 and His-CATB were purified using a GST-tag Protein Purification Kit (Beyotime) and a Ni-NTA 6FF Sefinose (TM) Resin Kit (BBI) according to the manufacturer's protocol respectively. The detailed pull-down assays were performed as previously described (Wang *et al.*, 2020b).

### Cell-free degradation assay

Purified recombinant proteins GST-SRL10, His-CATB and total proteins from 20-d-old seedlings of WYJ7 were used for cell-free degradation assay, and was carried out as previously described (Bello *et al.*, 2019; Lv *et al.*, 2014). The dilution for the mouse anti-GST antibody (TransGen Biotech) and the mouse anti-His antibody (TransGen Biotech) was 1:5000. Reactions were terminated at indicated time points, and the protein abundance was visualized via immune detection against anti-His and anti-GST. Total proteins from NIL-SRL10<sup>Hap1</sup> and NIL-SRL10<sup>Hap3</sup> were used for thermal stability analysis of protein and incubated under 28 °C and 42 °C for 0, 30, 60 and 90 min respectively. The dilution for the rabbit anti-SRL10 antibody was 1:10000.

### Bioinformatics analysis

RNA-seq and small RNA-seq analysis with three biological replicates was performed by Biomarker Technologies (<http://www.biomarker.com.cn/>) and Novogene (<https://www.novogene.com/>) respectively.

Single nucleotide polymorphisms (SNPs) in the genomic sequence of *SRL10* were extracted from 3025 sequences found on the Rice SNP-Seek Database (<https://snp-seek.irri.org/>) (Man-sueto *et al.*, 2017). The three main SNP genotypes were extracted for haplotype phenotypic analysis, and the rice materials were divided into three main subgroups: *aus*, *indica* and *japonica*.

### Construction of near-isogenic line

Based on the BC<sub>4</sub>F<sub>6</sub> chromosome segment substitution population of CJ16B which had experienced four generations of successive inbreeding with C84 as the recurrent parent, the lines carrying SRL10<sup>CJ16B</sup> (CSSLs-SRL10<sup>CJ16B</sup>) between marker C10-2 and C10-3 were screened out. The near-isogenic lines NIL-SRL10<sup>Hap1</sup> (carried CJ16B) and NIL-SRL10<sup>Hap3</sup> (carried C84) were constructed by using CSSLs-SRL10<sup>CJ16B</sup> backcrossed with C84 for two generations followed by inbreeding, then used for the treatment and yield test.

### Quantification and statistical analysis

Quantification analyses on all the measurements were conducted in GraphPad Prism 8. Data are presented with mean ± standard deviations. Significant difference was examined by Student's *t* test and Duncan's multiple range test.

### Author contributions

QQ and GZ designed the research. JW, JX, LW, MZ, JN, MC, XL, ZW, XL, JC, YL, ZZ, DZ, JH, LZ, GD, DR, ZG, LS, QZ, QL, LG and SY performed the research. QQ, GZ, JW and JX analysed the data. GZ, JW and JX wrote the paper.

### Acknowledgements

This work was supported by grants from the National Natural Science Foundation of China (32188102, 31861143006 and 31901483), Hainan Provincial key scientific research project, STP program from Hainan Yazhouwan Seed Laboratory (B21HJ0220-02) and Special Support Program(NKYCLJ-C-2021-015) and Nanfan special project (ZDXM06) of CAAS. We thank Prof. Jian Zhang and Dr. Yifeng Wang (CNRRI) for their help in the experiment of protein.

### Conflict of interest

The authors declare no conflict of interest.

### References

- Aparecido, L., Woo, S., Suazo, C., Hultine, K.R. and Blonder, B. (2020) High water use in desert plants exposed to extreme heat. *Ecol. Lett.* **23**, 1189–1200.
- Bartel, B. and Bartel, D.P. (2003) MicroRNAs: at the root of plant development? *Plant Physiol.* **132**, 709–717.
- Bello, B.K., Hou, Y., Zhao, J., Jiao, G., Wu, Y., Li, Z., Wang, Y. *et al.* (2019) NF-YB1-YC12-bHLH144 complex directly activates *Wx* to regulate grain quality in rice (*Oryza sativa* L.). *Plant Biotechnol. J.* **17**, 1222–1235.
- Biswas, M.S., Fukaki, H., Mori, I.C., Nakahara, K. and Mano, J. (2019) Reactive oxygen species and reactive carbonyl species constitute a feed-forward loop in auxin signaling for lateral root formation. *Plant J.* **100**, 536–548.
- Burd, C.G. and Dreyfuss, G. (1994) Conserved structures and diversity of functions of RNA-binding proteins. *Science* **265**, 615–621.
- Carrie, C., Small, I. (2012) A reevaluation of dual-targeting of proteins to mitochondria and chloroplasts. *Biochim. Biophys. Acta.* **1833**, 253–259.

- Chen, F., Dong, G., Wang, F., Shi, Y., Zhu, J., Zhang, Y., Ruan, B. et al. (2021) A  $\beta$ -ketoacyl carrier protein reductase confers heat tolerance via the regulation of fatty acid biosynthesis and stress signaling in rice. *New Phytol.* **232**, 655–672.
- Chen, K., Guo, T., Li, X.M., Zhang, Y.M., Yang, Y.B., Ye, W.W., Dong, N.Q. et al. (2019a) Translational regulation of plant response to high temperature by a Dual-Function tRNA<sup>His</sup>Guanylyltransferase in Rice. *Mol. Plant* **12**, 1123–1142.
- Chen, T., Chen, Z., Sathe, A.P., Zhang, Z.H., Li, L.J., Shang, H.H., Tang, S.Q. et al. (2019b) Characterization of a novel gain-of-function spotted-leaf mutant with enhanced disease resistance in rice. *Rice Sci.* **26**, 12.
- Crawford, A.J., McLachlan, D.H., Hetherington, A.M. and Franklin, K.A. (2012) High temperature exposure increases plant cooling capacity. *Curr. Biol.* **22**, R396–R397.
- Du, F., Guan, C. and Jiao, Y. (2018) Molecular mechanisms of leaf morphogenesis. *Mol. Plant* **11**, 1117–1134.
- Eamens, A.L., Kim, K.W., Curtin, S.J. and Waterhouse, P.M. (2012) DRB2 is required for microRNA biogenesis in *Arabidopsis thaliana*. *PLoS one* **7**, e35933.
- Fang, J., Guo, T., Xie, Z., Chun, Y., Zhao, J., Peng, L., Zafar, S.A. et al. (2021) The URL1-ROC5-TPL2 transcriptional repressor complex represses the *ACL1* gene to modulate leaf rolling in rice. *Plant Physiol.* **185**, 1722–1744.
- Fang, L., Zhao, F., Cong, Y., Sang, X., Du, Q., Wang, D., Li, Y. et al. (2012) Rolling-leaf 14 is a 2OG-Fe (II) oxygenase family protein that modulates rice leaf rolling by affecting secondary cell wall formation in leaves. *Plant Biotechnol. J.* **10**, 524–532.
- Fouracre, J.P. and Poethig, R.S. (2016) The role of small RNAs in vegetative shoot development. *Curr. Opin. Plant Biol.* **29**, 64–72.
- Foyer, C.H., Bloom, A.J., Queval, G. and Noctor, G. (2009) Photorespiratory metabolism: genes, mutants, energetics, and redox signaling. *Annu. Rev. Plant Biol.* **60**, 455–484.
- Fu, X., Xu, J., Zhou, M., Chen, M., Shen, L., Li, T., Zhu, Y. et al. (2019) Enhanced expression of QTL *qLL9/DEP1* facilitates the improvement of leaf morphology and grain yield in rice. *Int. J. Mol. Sci.* **20**, 866.
- Fujisawa, Y., Kato, T., Ohki, S., Ishikawa, A., Kitano, H., Sasaki, T., Asahi, T. et al. (1999) Suppression of the heterotrimeric G protein causes abnormal morphology, including dwarfism, in rice. *Proc. Natl. Acad. Sci. U. S. A.* **96**, 7575–7580.
- Gao, M., He, Y., Yin, X., Zhong, X., Yan, B., Wu, Y., Chen, J. et al. (2021) Ca<sup>2+</sup> sensor-mediated ROS scavenging suppresses rice immunity and is exploited by a fungal effector. *Cell* **184**, 5391–5404.
- Gao, X., Yuan, H.M., Hu, Y.Q., Li, J. and Lu, Y.T. (2014) Mutation of *Arabidopsis CATALASE2* results in hyponastic leaves by changes of auxin levels. *Plant Cell Environ.* **37**, 175–188.
- Guo, W., Chen, L., Herrera-Estrella, L., Cao, D. and Tran, L.P. (2020) Altering plant architecture to improve performance and resistance. *Trends Plant Sci.* **25**, 1154–1170.
- Guo, Z., Liu, X., Zhang, B., Yuan, X., Xing, Y., Liu, H., Luo, L. et al. (2021) Genetic analyses of lodging resistance and yield provide insights into post-Green-Revolution breeding in rice. *Plant Biotechnol. J.* **19**, 814–829.
- Haddad, N., Choukri, H., Ghanem, M.E., Smouni, A., Mentag, R., Rajendran, K., Hejaoui, K. et al. (2021) High-temperature and drought stress effects on growth, yield and nutritional quality with transpiration response to vapor pressure deficit in *Lentil*. *Plan. Theory* **11**, 95.
- Hasson, A., Blein, T. and Laufs, P. (2010) Leaving the meristem behind: the genetic and molecular control of leaf patterning and morphogenesis. *C. R. Biol.* **333**, 350–360.
- Hiraguri, A., Itoh, R., Kondo, N., Nomura, Y., Aizawa, D., Murai, Y., Koiwa, H. et al. (2005) Specific interactions between Dicer-like proteins and HYL1/DRB-family dsRNA-binding proteins in *Arabidopsis thaliana*. *Plant Mol. Biol.* **57**, 173–188.
- Huang, X., Qian, Q., Liu, Z., Sun, H., He, S., Luo, D., Xia, G. et al. (2009) Natural variation at the *DEP1* locus enhances grain yield in rice. *Nat. Genet.* **41**, 494–497.
- Jangam, A.P., Pathak, R.R. and Raghuram, N. (2016) Microarray analysis of rice *d1* (*RGA1*) mutant reveals the potential role of G-Protein alpha subunit in regulating multiple abiotic stresses such as drought, salinity, heat, and cold. *Front. Plant Sci.* **7**, 11.
- Jefferson, R.A., Kavanagh, T.A. and Bevan, M.W. (1987) GUS fusions: beta-glucuronidase as a sensitive and versatile gene fusion marker in higher plants. *EMBO J.* **6**, 3901–3907.
- Kan, Y., Mu, X.R., Zhang, H., Gao, J., Shan, J.X., Ye, W.W. and Lin, H.X. (2022) *TT2* controls rice thermotolerance through SCT1-dependent alteration of wax biosynthesis. *Nat. Plants* **8**, 53–67.
- Li, C., Zou, X., Zhang, C., Shao, Q., Liu, J., Liu, B., Li, H. et al. (2016a) *OsLBD3-7* overexpression induced adaxially rolled leaves in rice. *PLoS one* **11**, e0156413.
- Li, G., Zhang, C., Zhang, G., Fu, W., Feng, B., Chen, T., Peng, S. et al. (2020) Abscisic acid negatively modulates heat tolerance in rolled leaf rice by increasing leaf temperature and regulating energy homeostasis. *Rice* **13**, 18.
- Li, L., Shi, Z.Y., Li, L., Shen, G.Z., Wang, X.Q., An, L.S. and Zhang, J.L. (2010) Overexpression of *ACL1* (*abaxially curled leaf 1*) increased bulliform cells and induced abaxial curling of leaf blades in rice. *Mol. Plant* **3**, 807–817.
- Li, W.Q., Zhang, M.J., Gan, P.F., Qiao, L., Yang, S.Q., Miao, H., Wang, G.F. et al. (2017) *CLD1/SRL1* modulates leaf rolling by affecting cell wall formation, epidermis integrity and water homeostasis in rice. *Plant J.* **92**, 904–923.
- Li, X., Liao, M., Huang, J., Xu, Z., Lin, Z., Ye, N., Zhang, Z. et al. (2021) Glycolate oxidase-dependent H<sub>2</sub>O<sub>2</sub> production regulates IAA biosynthesis in rice. *BMC Plant Biol.* **21**, 326.
- Li, X.M., Chao, D.Y., Wu, Y., Huang, X., Chen, K., Cui, L.G., Su, L. et al. (2015) Natural alleles of a *proteasome  $\alpha 2$  subunit* gene contribute to thermotolerance and adaptation of African rice. *Nat. Genet.* **47**, 827–833.
- Li, Y., Yang, Y., Liu, Y., Li, D., Zhao, Y., Li, Z., Liu, Y. et al. (2019) Overexpression of *OsAGO1b* induces adaxially rolled leaves by affecting leaf abaxial sclerenchymatous cell development in rice. *Rice* **12**, 60.
- Li, Y.Y., Shen, A., Xiong, W., Sun, Q.L., Luo, Q., Song, T., Li, Z.L. et al. (2016b) Overexpression of *OsHox32* results in pleiotropic effects on plant type architecture and leaf development in rice. *Rice* **9**, 46.
- Liang, Y. and Li, Z. (2022) Split-Luciferase complementation for analysis of virus-host protein interactions. *Methods Mol. Biol.* **2400**, 55–62.
- Lin, H., Chen, Y., Zhang, H., Fu, P. and Fan, Z. (2017) Stronger cooling effects of transpiration and leaf physical traits of plants from a hot dry habitat than from a hot wet habitat. *Funct. Ecol.* **31**, 2202–2211.
- Liu, B., Li, P., Li, X., Liu, C., Cao, S., Chu, C. and Cao, X. (2005) Loss of function of *OsDCL1* affects microRNA accumulation and causes developmental defects in rice. *Plant Physiol.* **139**, 296–305.
- Liu, C., Zheng, S., Gui, J., Fu, C., Yu, H., Song, D., Shen, J. et al. (2018) Shortened basal internodes encodes a gibberellin 2-Oxidase and contributes to lodging resistance in rice. *Mol. Plant* **11**, 288–299.
- Liu, X., Li, M., Liu, K., Tang, D., Sun, M., Li, Y., Shen, Y. et al. (2016) *Semi-Rolled Leaf 2* modulates rice leaf rolling by regulating abaxial side cell differentiation. *J. Exp. Bot.* **67**, 2139–2150.
- Lu, C. and Fedoroff, N. (2000) A mutation in the *Arabidopsis HYL1* gene encoding a dsRNA binding protein affects responses to abscisic acid, auxin, and cytokinin. *Plant Cell* **12**, 2351–2366.
- Lu, C.A., Lin, C.C., Lee, K.W., Chen, J.L., Huang, L.F., Ho, S.L., Liu, H.J. et al. (2007) The SnRK1A protein kinase plays a key role in sugar signaling during germination and seedling growth of rice. *Plant Cell* **19**, 2484–2499.
- Lu, Z., Yu, H., Xiong, G., Wang, J., Jiao, Y., Liu, G., Jing, Y. et al. (2013) Genome-wide binding analysis of the transcription activator ideal plant architecture1 reveals a complex network regulating rice plant architecture. *Plant Cell* **25**, 3743–3759.
- Lv, Q., Zhong, Y., Wang, Y., Wang, Z., Zhang, L., Shi, J., Wu, Z. et al. (2014) *SPX4* negatively regulates phosphate signaling and homeostasis through its interaction with *PHR2* in rice. *Plant Cell* **26**, 1586–1597.
- Ma, X., Zhang, Q., Zhu, Q., Liu, W., Chen, Y., Qiu, R., Wang, B. et al. (2015) A robust CRISPR/Cas9 system for convenient, high-efficiency multiplex genome editing in monocot and dicot plants. *Mol. Plant* **8**, 1274–1284.
- Ma, Y., Zhao, Y., Shangguan, X., Shi, S., Zeng, Y., Wu, Y., Chen, R. et al. (2017) Overexpression of *OsRRK1* changes leaf morphology and defense to insect in rice. *Front. Plant Sci.* **8**, 1783.
- Mansueto, L., Fuentes, R.R., Borja, F.N., Detras, J., Abriol-Santos, J.M., Chebotarov, D., Sanciangco, M. et al. (2017) Rice SNP-seek database update: new SNPs, indels, and queries. *Nucleic Acids Res.* **45**, d1075–d1081.

- Matsumura, T., Tabayashi, N., Kamagata, Y., Souma, C. and Saruyama, H. (2002) Wheat catalase expressed in transgenic rice can improve tolerance against low temperature stress. *Physiol. Plant* **116**, 317–327.
- Mhamdi, A., Noctor, G. and Baker, A. (2012) Plant catalases: peroxisomal redox guardians. *Arch. Biochem. Biophys.* **525**, 181–194.
- Mittler, R., Finka, A. and Goloubinoff, P. (2012) How do plants feel the heat? *Trends Biochem. Sci.* **37**, 118–125.
- Moon, J. and Hake, S. (2011) How a leaf gets its shape. *Curr. Opin. Plant Biol.* **14**, 24–30.
- Nogueira, F.T., Madi, S., Chitwood, D.H., Juarez, M.T. and Timmermans, M.C. (2007) Two small regulatory RNAs establish opposing fates of a developmental axis. *Genes Dev.* **21**, 750–755.
- Pegler, J.L., Oultram, J., Grof, C. and Eamens, A.L. (2019) Profiling the abiotic stress responsive microRNA landscape of *Arabidopsis thaliana*. *Plan. Theory* **8**, 58.
- Pegler, J.L., Oultram, J., Grof, C. and Eamens, A.L. (2020) Molecular Manipulation of the miR399/PHO2 expression module alters the salt stress response of *Arabidopsis thaliana*. *Plan. Theory* **10**, 73.
- Qiu, Z., Chen, D., He, L., Zhang, S., Yang, Z., Zhang, Y., Wang, Z. et al. (2018) The rice *white green leaf 2* gene causes defects in chloroplast development and affects the plastid ribosomal protein S9. *Rice* **11**, 39.
- Qiu, Z., Zhu, L., He, L., Chen, D., Zeng, D., Chen, G., Hu, J. et al. (2019) DNA damage and reactive oxygen species cause cell death in the rice *local lesions 1* mutant under high light and high temperature. *New Phytol.* **222**, 349–365.
- Raghuram, B., Sheikh, A.H., Rustagi, Y. and Sinha, A.K. (2015) MicroRNA biogenesis factor DRB1 is a phosphorylation target of mitogen activated protein kinase MPK3 in both rice and *Arabidopsis*. *FEBS J.* **282**, 521–536.
- Ray, D.K., Gerber, J.S., MacDonald, G.K. and West, P.C. (2015) Climate variation explains a third of global crop yield variability. *Nat. Commun.* **6**, 5989.
- Ruan, B., Shang, L., Zhang, B., Hu, J., Wang, Y., Lin, H., Zhang, A. et al. (2020) Natural variation in the promoter of *TGW2* determines grain width and weight in rice. *New Phytol.* **227**, 629–640.
- Sakaguchi, J. and Watanabe, Y. (2012) MiR165/166 and the development of land plants. *Dev. Growth Differ.* **54**, 93–99.
- Singleton, C., Howard, T.P. and Smirnov, N. (2014) Synthetic metabolons for metabolic engineering. *J. Exp. Bot.* **65**, 1947–1954.
- Small, I., Wintz, H., Akashi, K. and Mireau, H. (1998) Two birds with one stone: genes that encode products targeted to two or more compartments. *Plant Mol. Biol.* **38**, 265–277.
- Song, X., Li, P., Zhai, J., Zhou, M., Ma, L., Liu, B., Jeong, D.H. et al. (2012) Roles of *DCL4* and *DCL3b* in rice phased small RNA biogenesis. *Plant J.* **69**, 462–474.
- Springer, N. (2010) Shaping a better rice plant. *Nat. Genet.* **42**, 475–476.
- Sun, J., Cui, X., Teng, S., Kunngong, Z., Wang, Y., Chen, Z., Sun, X. et al. (2020) HD-ZIP IV gene *Roc8* regulates the size of bulliform cells and lignin content in rice. *Plant Biotechnol. J.* **18**, 2559–2572.
- Sun, L., Zhang, Q., Wu, J., Zhang, L., Jiao, X., Zhang, S., Zhang, Z. et al. (2014) Two rice authentic histidine phosphotransfer proteins, OsAHP1 and OsAHP2, mediate cytokinin signaling and stress responses in rice. *Plant Physiol.* **165**, 335–345.
- Tang, Y., Gao, C.C., Gao, Y., Yang, Y., Shi, B., Yu, J.L., Lyu, C. et al. (2020) OsNSUN2-mediated 5-methylcytosine mRNA modification enhances rice adaptation to high temperature. *Dev. Cell* **53**, 272–286.
- Tanz, S.K., Castleden, I., Small, I.D., Millar, A.H. (2013) Fluorescent protein tagging as a tool to define the subcellular distribution of proteins in plants. *Front Plant Sci.* **24**, 214.
- Thordal-Christensen, H., Zhang, Z., Wei, Y. and Collinge, D.B. (1997) Subcellular localization of H<sub>2</sub>O<sub>2</sub> in plants. H<sub>2</sub>O<sub>2</sub> accumulation in papillae and hypersensitive response during the barley—powdery mildew interaction. *Plant J.* **11**, 1187–1194.
- Tian, J., Wang, C., Xia, J., Wu, L., Xu, G., Wu, W., Li, D. et al. (2019) Teosinte ligule allele narrows plant architecture and enhances high-density maize yields. *Science* **365**, 658–664.
- Toki, S., Hara, N., Ono, K., Onodera, H., Tagiri, A., Oka, S. and Tanaka, H. (2006) Early infection of scutellum tissue with *Agrobacterium* allows high-speed transformation of rice. *Plant J.* **47**, 969–976.
- Vu, L.D., Gevaert, K. and De Smet, I. (2019) Feeling the heat: Searching for plant thermosensors. *Trends Plant Sci.* **24**, 210–219.
- Wang, J., Wang, R., Fang, H., Zhang, C., Zhang, F., Hao, Z., You, X. et al. (2021a) Two VOZ transcription factors link an E3 ligase and an NLR immune receptor to modulate immunity in rice. *Mol. Plant* **14**, 253–266.
- Wang, J.J., Xu, J., Qian, Q. and Zhang, G.H. (2020a) Development of Rice Leaves: How histocytes modulate leaf polarity establishment. *Rice Sci.* **27**, 468–479.
- Wang, L., Ming, L., Liao, K., Xia, C., Sun, S., Chang, Y., Wang, H. et al. (2021b) Bract suppression regulated by the miR156/529-SPLs-NL1-PLA1 module is required for the transition from vegetative to reproductive branching in rice. *Mol. Plant* **14**, 1168–1184.
- Wang, Y., Hou, Y., Qiu, J., Wang, H., Wang, S., Tang, L., Tong, X. et al. (2020b) Abscisic acid promotes jasmonic acid biosynthesis via a 'SAPK10-bZIP7. *New Phytol.* **228**, 1336–1353.
- Wang, Y. and Li, J. (2005) The plant architecture of rice (*Oryza sativa*). *Plant Mol. Biol.* **59**, 75–84.
- Waterhouse, P.M., Wang, M.B. and Lough, T. (2001) Gene silencing as an adaptive defence against viruses. *Nature* **411**, 834–842.
- Woo, Y.M., Park, H.J., Su'udi, M., Yang, J.I., Park, J.J., Back, K., Park, Y.M. et al. (2007) *Constitutively wilted 1*, a member of the rice YUCCA gene family, is required for maintaining water homeostasis and an appropriate root to shoot ratio. *Plant Mol. Biol.* **65**, 125–136.
- Xiang, J.J., Zhang, G.H., Qian, Q. and Xue, H.W. (2012) *Semi-rolled leaf 1* encodes a putative glycosylphosphatidylinositol-anchored protein and modulates rice leaf rolling by regulating the formation of bulliform cells. *Plant Physiol.* **159**, 1488–1500.
- Xu, J., Wang, J.J., Xue, H.W. and Zhang, G.H. (2021) Leaf direction: Lamina joint development and environmental responses. *Plant Cell Environ.* **44**, 2441–2454.
- Xu, P., Ali, A., Han, B. and Wu, X. (2018) Current advances in molecular basis and mechanisms regulating leaf morphology in Rice. *Front. Plant Sci.* **9**, 1528.
- Xu, Y., Zhang, L., Ou, S., Wang, R., Wang, Y., Chu, C. and Yao, S. (2020) Natural variations of *SLG1* confer high-temperature tolerance in *indica* rice. *Nat. Commun.* **11**, 5441.
- Ye, N., Zhu, G., Liu, Y., Li, Y. and Zhang, J. (2011) ABA controls H<sub>2</sub>O<sub>2</sub> accumulation through the induction of *OsCATB* in rice leaves under water stress. *Plant Cell Physiol.* **52**, 689–698.
- Yu, C., Wang, L., Chen, C., He, C., Hu, J., Zhu, Y. and Huang, W. (2014) Protoplast: a more efficient system to study nucleo-cytoplasmic interactions. *Biochem. Biophys. Res. Commun.* **450**, 1575–1580.
- Zhang, D., Liu, M., Tang, M., Dong, B., Wu, D., Zhang, Z. and Zhou, B. (2015a) Repression of microRNA biogenesis by silencing of *OsDCL1* activates the basal resistance to *Magnaporthe oryzae* in rice. *Plant Sci.* **237**, 24–32.
- Zhang, G., Hou, X., Wang, L., Xu, J., Chen, J., Fu, X., Shen, N. et al. (2021a) *PHOTO-SENSITIVE LEAF ROLLING 1* encodes a polygalacturonase that modifies cell wall structure and drought tolerance in rice. *New Phytol.* **229**, 890–901.
- Zhang, G.H., Xu, Q., Zhu, X.D., Qian, Q. and Xue, H.W. (2009) SHALLOT-LIKE1 is a KANADI transcription factor that modulates rice leaf rolling by regulating leaf abaxial cell development. *Plant Cell* **21**, 719–735.
- Zhang, J., Zhang, H., Srivastava, A.K., Pan, Y., Bai, J., Fang, J., Shi, H., and Zhu, J.K. (2018) Knockdown of rice MicroRNA166 confers drought resistance by causing leaf rolling and altering stem xylem development. *Plant Physiol.* **176**, 2082–2094.
- Zhang, J.J., Wu, S.Y., Jiang, L., Wang, J.L., Zhang, X., Guo, X.P., Wu, C.Y. et al. (2015b) A detailed analysis of the leaf rolling mutant *slr2* reveals complex nature in regulation of bulliform cell development in rice (*Oryza sativa* L.). *Plant Biol.* **17**, 437–448.
- Zhang, T., You, J., Zhang, Y., Yao, W., Chen, W., Duan, Q., Xiao, W. et al. (2021b) *LF1* regulates the lateral organs polarity development in rice. *New Phytol.* **231**, 1265–1277.
- Zhang, Y.H. (2011) Substrate channeling and enzyme complexes for biotechnological applications. *Biotechnol. Adv.* **29**, 715–725.
- Zhang, Z., Xu, Y., Xie, Z., Li, X., He, Z.H. and Peng, X.X. (2016) Association-dissociation of glycolate oxidase with catalase in rice: a potential switch to modulate intracellular H<sub>2</sub>O<sub>2</sub> levels. *Mol. Plant* **9**, 737–748.
- Zhong, H. and Läuchli, A. (1993) Changes of cell wall composition and polymer size in primary roots of cotton seedlings under high salinity. *J. Exp. Bot.* **44**, 773–778.

- Zhou, Y., Wang, D., Wu, T., Yang, Y., Liu, C., Yan, L., Tang, D. et al. (2018) LRRK1, a receptor-like cytoplasmic kinase, regulates leaf rolling through modulating bulliform cell development in rice. *Mol. Breeding* **38**, 48.
- Zhu, Y., Li, T., Xu, J., Wang, J., Wang, L., Zou, W., Zeng, D. et al. (2020) Leaf width gene *LW5/D1* affects plant architecture and yield in rice by regulating nitrogen utilization efficiency. *Plant Physiol. Biochem.* **157**, 359–369.
- Zou, L.P., Sun, X.H., Zhang, Z.G., Liu, P., Wu, J.X., Tian, C.J., Qiu, J.L. et al. (2011) Leaf rolling controlled by the homeodomain leucine zipper class IV gene *Roc5* in rice. *Plant Physiol.* **156**, 1589–1602.

## Supporting information

Additional supporting information may be found online in the Supporting Information section at the end of the article.

**Figure S1** Transcriptomic analysis in leaves of WYJ7 and *sr110*.

**Figure S2** Overexpression lines of *SRL10*.

**Figure S3** Confirmation of the CRISPR/Cas9 transgenic lines of *SRL10*.

**Figure S4** Phylogenic and conservative analysis of *SRL10*.

**Figure S5** Scanning of interacting proteins of *SRL10*.

**Figure S6** The relative expression level analysis of miRNAs in plants.

**Figure S7** Subcellular localization of CATB and bimolecular fluorescence complementation assay.

**Table S1** Genetic analysis of F<sub>2</sub> population of hybrid combination.

**Table S2** Primers used for map-based cloning.

**Table S3** Primers used for sequencing.

**Table S4** Primers used for vector construction.

**Table S5** Primers used for qRT-PCR.

**Table S6** Accession lines of different haplotypes used for analysing of high temperature response and 2 years' heading date of these lines.